โครงการการเรียนการสอนเพื่อเสริมประสบการณ์

การสำรวจพื้นที่ศักยภาพแหล่งแร่ทองคำ โดยใช้ภาพถ่ายดาวเทียม ASTER บริเวณเหมืองทองคำชาตรี จังหวัดพิจิตรและเพชรบูรณ์

โดย

นายศิกวัส ศรีประภาพร

เลขประจำตัวนิสิต 5732750323

โครงการนี้เป็นส่วนหนึ่งของการศึกษาระดับปริญญาตรี
ภาควิชาธรณีวิทยา คณะวิทยาศาสตร์ จุฬาลงกรณ์มหาวิทยาลัย
ปีการศึกษา 2560

การสำรวจพื้นศักยภาพแหล่งแร่ทองคำโดยใช้ภาพถ่ายดาวเทียม ASTER บริเวณเหมืองทองคำชาตรี จังหวัดพิจิตรและเพชรบูรณ์

นายศิกวัส ศรีประภาพร

รายงานฉบับนี้เป็นส่วนหนึ่งของการศึกษาตามหลักสูตรปริญญาวิทยาศาสตรบัณฑิต
ภาควิชาธรณีวิทยา คณะวิทยาศาสตร์ จุฬาลงกรณ์มหาวิทยาลัย
ปีการศึกษา 2560

DETECING HIGH-POTENTIAL GOLD MINERALIZATION AREAS USING ASTER SATELLITE IMAGES AT CHATREE GOLD MINING AREA, PHICHIT AND PHETHCHABUN PROVINCES

MR. SIGAWAS SRIPRAPAPORN

A REPORT SUBMITTED IN PARTIAL FULFILLMENT OF THE REQUIREMENTS
FOR THE DEGREE OF THE BACHELOR OF SCIENCE PROGRAM IN GEOLOGY
DEPARTMENT OF GEOLOGY
FACULTY OF SCIENCE
CHULALONGKORN UNIVERSITY
ACADEMIC YEAR 2017

Title: DETECING HIGH-POTENTIAL GOLD MINERALIZATION AREAS USING ASTER SATELLITE IMAGES AT CHATREE GOLD MINING AREA, PHICHIT AND PHETHCHABUN PROVINCES

Researcher: Mr. Sigawas Sriprapaporn

Advisor: Dr. Abhisit Salam

Co-advisor: Dr. Sumet Phantuwongraj

Date of submission

_____/_____/_____

Date of approval

_____/_____/_____

Signature _____

(Dr. Abhisit Salam)

Senior Project's Advisor

หัวข้องานวิจัย: การสำรวจพื้นศักยภาพแหล่งแร่ทองคำโดยใช้ภาพถ่ายดาวเทียม ASTER บริเวณเหมืองทองคำชาตรี จังหวัดพิจิตรและเพชรบูรณ์

ผู้ทำการวิจัย: นายศิกวัส ศรีประภาพร รหัสประจำตัวนิสิต: 5732750323

อาจารย์ที่ปรึกษา: ดร. อภิสิทธิ์ ซาลำ

อาจารย์ที่ปรึกษาร่วม: ดร.สุเมธ พันธุวงค์ราช

ภาควิชา: ธรณีวิทยา

ปีการศึกษา: 2560

บทคัดย่อ

ภาพถ่ายดาวเทียมสามารถนำมาใช้ในการสำรวจและจัดการทรัพยากรต่าง ๆ บนผิวโลก ไม่ว่าจะเป็นพื้นที่ป่าไม้ การวางแผนการใช้ที่ดินและการสำรวจทางธรณีวิทยา หนึ่งในภาพถ่ายดาวเทียมที่ถูกใช้อย่างแพร่หลาย คือ ภาพถ่ายดาวเทียม ASTER (Advanced Spaceborne Thermal Emission and Reflection Radiometer) ซึ่งใช้ในการสำรวจแหล่งแร่ทองคำ โดยอาศัยค่าการสะท้อนแสงที่บันทึกได้ของวัตถุบนผิวดินในช่วงความยาวคลื่นแสงตามองเห็น อินฟราเรดใกล้ อินฟราเรดคลื่นสั้นและอินฟราเรดความร้อน งานวิจัยนี้จึงมีวัตถุประสงค์เพื่อนำภาพถ่ายดาวเทียม ASTER ที่บันทึกข้อมูลภาพก่อนการเปิดกิจการของเหมืองทองคำชาตรีมาใช้ในการสำรวจพื้นที่ศักยภาพแหล่งแร่ทองคำ ทำการศึกษาการตรวจพบแร่แปรเปลี่ยนที่มีหมู่ไฮดรอกซิลในโครงสร้างบนผิวดินที่เกิดร่วมในแหล่งแร่ที่มีการสะสมตัวของทองคำแบบอีพิเทอร์มอลอุณหภูมิต่ำ ในบริเวณแหล่งแร่ทองคำชาตรี จังหวัดพิจิตรและเพชรบูรณ์ด้วยวิธี band ratio และ principal component analysis จากนั้นทำการแปลความหมายจากภาพถ่ายดาวเทียม ASTER และทำการเก็บตัวอย่างหินบริเวณผิวดิน นำมาวิเคราะห์ด้วยการศึกษาศิลาวรรณนาและศึกษาธรณีเคมีด้วยวิธี x-ray diffraction (XRD) ผลการศึกษาพบว่าภาพถ่ายดาวเทียม ASTER สามารถตรวจพบพื้นที่ศักยภาพแหล่งแร่ทองคำในบริเวณแหล่งแร่ทองคำชาตรีได้ร ซึ่งสอดคล้องกับผลการศึกษาด้วยศิลาวรรณาและธรณีเคมี ที่พบแร่แปรเปลี่ยนที่มีหมู่ไฮดรอกซิลในโครงสร้าง ได้แก่ อิลไลต์ เซอริไซต์ คลอไรต์ เคโอลิไนต์และมอนต์โมริลโลไนต์ จากการศึกษาในครั้งนี้สามารถเป็นต้นแบบในการค้นหาพื้นที่ศักยภาพแหล่งแร่ทองคำแบบอีพิเทอร์มอลอุณหภูมิต่ำในพื้นที่เขตร้อนชื้นอื่น ๆ ต่อไป

คำสำคัญ: ภาพถ่ายดาวเทียม ASTER, แร่แปรเปลี่ยน, แหล่งแร่ทองคำแบบอีพิเทอร์มอลอุณหภูมิต่ำ

Title: DETECING HIGH-POTENTIAL GOLD MINERALIZATION AREAS USING ASTER SATELLITE IMAGES AT CHATREE GOLD MINING AREA, PHICHIT AND PHETHCHABUN PROVINCES

Researcher: Mr. Sigawas Sriprapaporn **ID:** 5732750323

Advisor: Dr. Abhisit Salam

Co-advisor: Dr. Sumet Phantuwongraj

Department: Geology

Academic year: 2017

Abstract

Satellite imagery has been used for resource exploration and management on earth's surface such as wood density, land management and geological exploration. One of well-known satellite data, Advanced Spaceborne Thermal Emission and Reflection Radiometer (ASTER) satellite images, are used to observe gold deposits by collecting reflectance data of surface materials in the spectral ranges: visible, near-infrared, shortwave-infrared and thermal-infrared. The objective of this study is to use ASTER satellite images obtained before the official operation of Chatree gold mine to detect OH-bearing altered surface minerals considered high-potential gold mineralization areas. The image transformations: band ratio indices and principal component analysis were used on ASTER satellite images covering Chatree gold deposit. Subsequently, the ASTER data was compared to petrographic study and x-ray diffraction analysis of rock samples from representative locations. The results show ASTER satellite images can be used to detect high-potential gold mineralization when analyzed for OH-bearing altered minerals: illite, sericite, chlorite, and kaolinite and montmorillonite. According to the results, this research can be a case study for detecting high-potential gold mineralization areas for the low-sulfidation epithermal deposit in tropical regions.

Keywords: ASTER satellite images, alteration minerals, low-sulfidation epithermal gold deposit

ACKNOWLEDGEMENTS

I would like to thank my advisor, Dr. Abhisit Salam, for his inspiration and encouragement during this project. He provided the opportunity to access Chatree mining leases during the field study. Dr. Salam has given me guidance and motivation throughout my bachelor's degree at Chulalongkorn university. I would also like to thank my co-advisor, Dr. Sumet Phantuwongraj, for teaching satellite image transformation. I am thankful for my roommate, Graysen J. Ortega, for reviewing and editing drafts of my project report. This project was funded with financial and logistical support from the Department of Geology, Faculty of Science, Chulalongkorn University.

I would like to thank Akara Resources Public Company Limited for giving me access to the field areas and the private radiometric survey for high-potential gold mineralization map comparison that provides better discussion on using remote sensing for mineral exploration in tropical regions. Many thanks go to Khun Jiraprapa Niampan and Khun Banjong Puangthong, staff of the Department of Geology that gave advice and support in laboratory procedures. I also feel thankful for Sirawit Kaewpaluk and Smith Leknettip, senior students at the department, for helping me understand and review geology concepts during the project.

Finally, I would like to give great thanks to my family, who provide mental and financial support for my studies in Bangkok. I could not have finished this study at Chulalongkorn University without their belief in me and their kind support.

CONTENTS

LIST OF TABLES

Page

LIST OF FIGURES

Page

CHAPTER I

INTRODUCTION

1.1 RATIONALE

Gold in Thailand has been produced legally since the reign of King Rama. Today, gold is one of the main economic minerals of the country. Northern, eastern and southern Thailand are considered high-potential gold mineralization areas by the Thai Department of Mineral Resources, 2009. Thailand has two commercial gold mining operations: Tung Kum and Chatree. Chatree gold mine, one of largest gold mines in Thailand, is located in Phichit and Phetchabun provinces which was successful in exploration with 0.99 million ounces (oz) of ore reserve. Notably, Chatree gold mine is considered to have the lowest mine production cost of gold and silver and probably the lowest in the world (Salam, 2013).

At the Chatree gold mine, gold and silver were first confirmed in 1988 at Khao Mo in central Thailand where resistant isolated mountains remain due to widespread silicification (Diemar and Diemar, 1999). Conventional techniques such as soil geochemistry, mapping and trenching were used in the Khao Mo area for greenfield exploration (during the early exploration stage).

For universal greenfield exploration, stream sediments are collected in reconnaissance surveys to indicate ore zones and draw areas of interest. Rock samples and soil sediments usually are then collected for geochemical analysis in the detailed survey. In some cases, vegetation samples and vapor samples are also collected because surface soil can reflect the geology below.

After greenfield exploration, Khao Mo (A prospect) was recognized as a high-potential area for epithermal gold deposits. Exploration showed the country rock (volcanics) containing epithermal quartz vein with typical textures of low-sulfidation epithermal such as crustiform and colloform banding. Characteristics of Chatree gold-silver

deposit style present in veins, stockworks and minor breccias hosted by volcanic and volcanogenic sedimentary rocks (Salam et al., 2014).

Recently, new technologies have been developed for mineral exploration. One new technology has led to the development of remote sensing using satellite images in brownfield exploration. Remote sensing is considered an important role in mineral exploration locating alteration zones related to gold deposits (Gabr et al., 2010). Research shows, the average spectra for altered (mineralized and non-mineralized) rocks shows higher reflectance than unaltered rocks which is a crucial characteristic for band ratio transformation (Fig. 1.1).

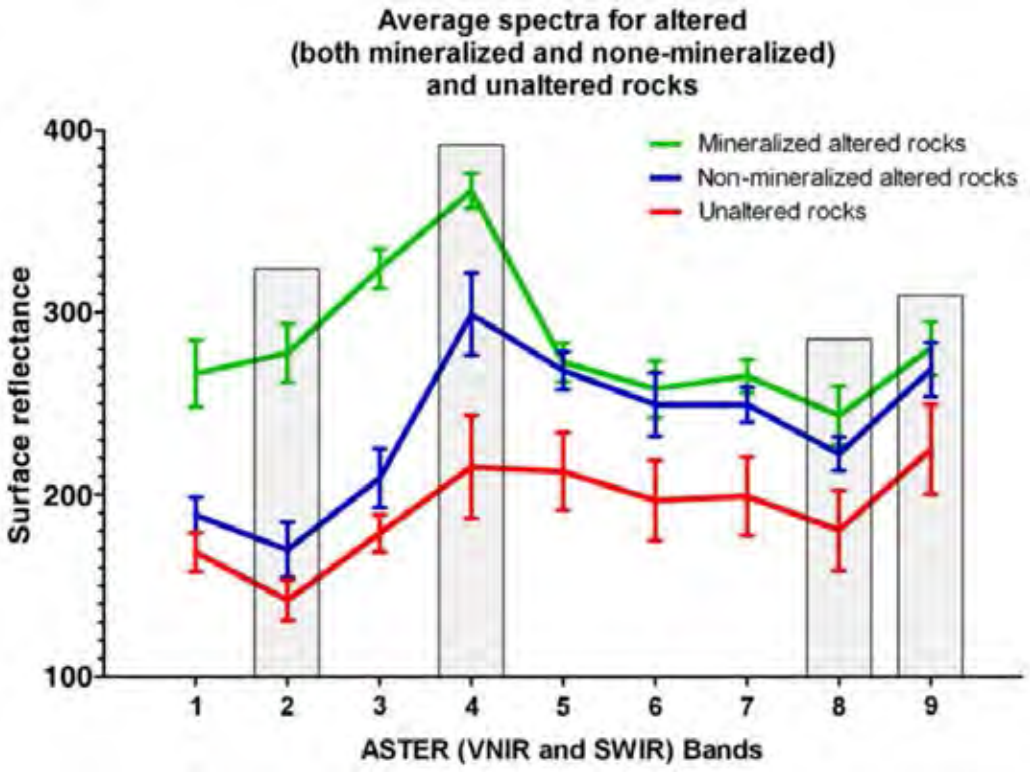

Fig. 1.1 Average spectra for altered (mineralized and non-mineralized) and unaltered rocks in Abu-Marawat, Red Sea Governorate, Egypt. Highlighted (gray bars) are the spectras used in the band ratio transformation (Gabr et al., 2010).

Band ratio is one of the popular image transformation used to identify specific objects on the surface. The mineralogic indices proposed by Ninomiya (2003) were applied to ASTER satellite images in Cuprite mining in Nevada, U.S.A. OH-bearing Altered Mineral Index (OHI), one of the mineralogic indices, quantifies the clay mineral density on the surface by measuring the difference between the clay mineral reflectance and absorption in the SWIR bands and the result agrees well to the geology of the area. Another well-known image transformation called Principal Component Analysis (PCA) is also used for alteration mapping. The ASTER imagery of the study area in Patagonia, Argentina using PCA can statistically distinguish the spectral data into specific alteration minerals such as alunite, illite and kaolinite composited into alteration mineral abundance images. The field study also corresponds to the processed satellite images (Crósta et al., 2003)

Table 1.1 ASTER sensor systems characteristics (Zhang et al., 2007).

ASTER Sensor Systems				
Sub-system	Band No.	Spectral Range (μm)	Spatial Resolution	bits
Visible Near Infrared (VNIR)	1	0.52 – 0.60	15m	8bits
	2	0.63 – 0.69		
	3N	0.78 – 0.86		
	3B	0.78 – 0.86		
Shortwave Infrared (SWIR)	4	1.600 – 1.700	30m	8bits
	5	2.145 – 2.185		
	6	2.185 – 2.225		
	7	2.235 – 2.285		
	8	2.295 – 2.365		
	9	2.360 – 2.430		
Thermal Infrared (TIR)	10	8.125 – 8.475	90m	12bits
	11	8.475 – 8.825		
	12	8.925 – 9.275		
	13	10.25 – 10.95		

Based on previous alteration study, remote sensing is used in brownfield exploration for Chatree gold deposit. The ASTER satellite images acquired on January 5, 2001 can be freely accessed from The U.S. National Aeronautics and Space Administration

(NASA) and processed through image transformations: band ratio and PCA. This project aims to use remote sensing for alteration mapping to better understand on mineral exploration in low-sulfidation epithermal gold deposit in Thailand.

1.1 OBJECTIVE

To detect OH-bearing altered minerals considered high-potential gold mineralization areas in low-sulfidation epithermal gold deposit using ASTER satellite images

1.3 STUDY AREA

The study area is located in northern Thailand covering Chatree gold mine (Fig. 1.2). The coordinates of the 100-square-kilometer area are 16° 20' 51.6"N, 100° 36' 23.4"E, 16° 20' 51.6"N, 100° 41' 57.5"E, 16° 15' 23.6"N, 100° 36' 23.4"E and 16° 15' 23.6"N, 100° 41' 57.5"E.

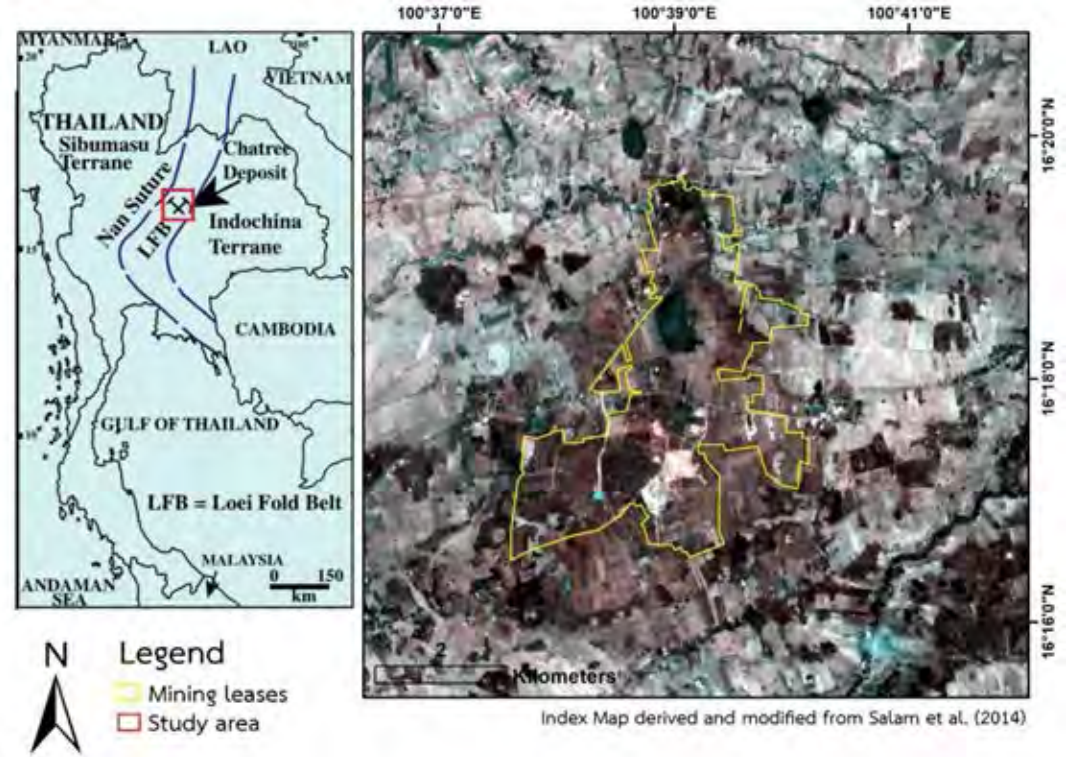

Fig. 1.2 ASTER satellite imagery with spectral band 2, 1, 1 in RGB showing location of the study area.

1.4 EXPECTED BENEFITS

1.4.1 High-potential gold mineralization map

1.4.2 The case study for detecting high-potential gold mineralization areas or the low-sulfidation epithermal deposit in tropical climates

1.4.3 The application for mineral exploration

1.5 LITERATURE REVIEWS

1.5.1 THE USING OF REMOTE SENSING FOR MINERAL EXPLORATION

A number of remote sensing investigations for mineral exploration and lithological mapping have been conducted worldwide (Pour et al., 2013). One application is to locate alteration zones related to gold deposits in Egypt which corresponds to the collected samples (Gabr et al., 2010). Another remote sensing study in Bau gold district, Borneo island covered with dense and often complete vegetation reveals the detection for clay minerals and iron-rich minerals by using band ratio and principal component analysis for alteration mapping (Pour et al., 2013).

1.5.2 SATELLITE IMAGE TRANSFORMATION

1.5.2.1 Band Ratio

Band ratio images have spectral enhancement by dividing the digital number values in one spectral band by the corresponding values in another band. Image results show the characteristics of the image features, regardless of variations in the scene condition. A band ratio image effectively compensates for the brightness variation caused by the varying topography and emphasizes the color content of the image data. Band ratio images are effective for mineral mapping as they enhance

compositional variations. However, the band ratio technique does not indicate the occurrence of a mineral with absolute quantity, so ground follow-ups and proper thresholding is necessary (Fatima et al., 2017).

1.5.2.2 Principal Component Analysis

The principal component transformation is a multivariate statistical technique selecting uncorrelated linear combinations or eigenvector loadings of variables that each successively extracted linear combination or principal component (PC) has a smaller variance. The main aim of PC analysis is to remove excessiveness in multispectral information. Principal component analysis is widely used for alteration mapping in metallogenic provinces (Boloki and Poormirzaee, 2010).

CHAPTER II

GEOLOGICAL SETTING

2.1 INTRODUCTION

The origin of Chatree gold deposit is mainly described in this chapter from regional to local geology**.** The Chatree gold deposit is located in Loei Fold Belt considered commercially for precious metals. The geology of Chatree gold deposit is also described in the final part showing the characteristics of depositional geological structure.

2.2 REGIONAL GEOLOGY

A number of terranes are the composition of Southeast Asia region considered controversially for the tectonic evolution due to the complexity of the area. However, a number of studies agree to the main idea that Thailand is formed with two major tectonic terranes: Shan-Thai in the west and Indochina terrane in the east (Fig. 2.1). The Shan-Thai terrane consists of east Myanmar, western Thailand, western Malaysia Peninsular and Sumatra. The Indochina plate consists of Eastern Thailand, Laos, Cambodia and Vietnam. These terranes are divided by Sukhothai Fold Belt (SFB) and also known as Sukhothai Arc on the west and Loei Fold Belt (LFB) elongated from the north to the south. These two belts are considered to be the most potential zone for mineral deposits in the region (Salam et al., 2014).

Loei Fold Belt has a complex magmatic history and widespread of Permo-Triassic magmatism, based on geochronology (e.g. U-Pb zircon ages dating and other techniques) and whole rock geochemistry, mainland Southeast Asia, for both in SFB and LFB, occurred subsequently of subduction-related magmatism (Salam, 2013), which is accompanied by major mineralization including precious metals such as gold, silver, copper, and iron (Fig. 2.1). The belt is extended from Lao PDR (People's Democratic Republic) through provinces

in the northeast of Thailand: Loei, Phichit, and Phetchabun in central Thailand along the edge of Khorat plateau to eastern Thailand and possibly to Cambodia (Fig. 2.2).

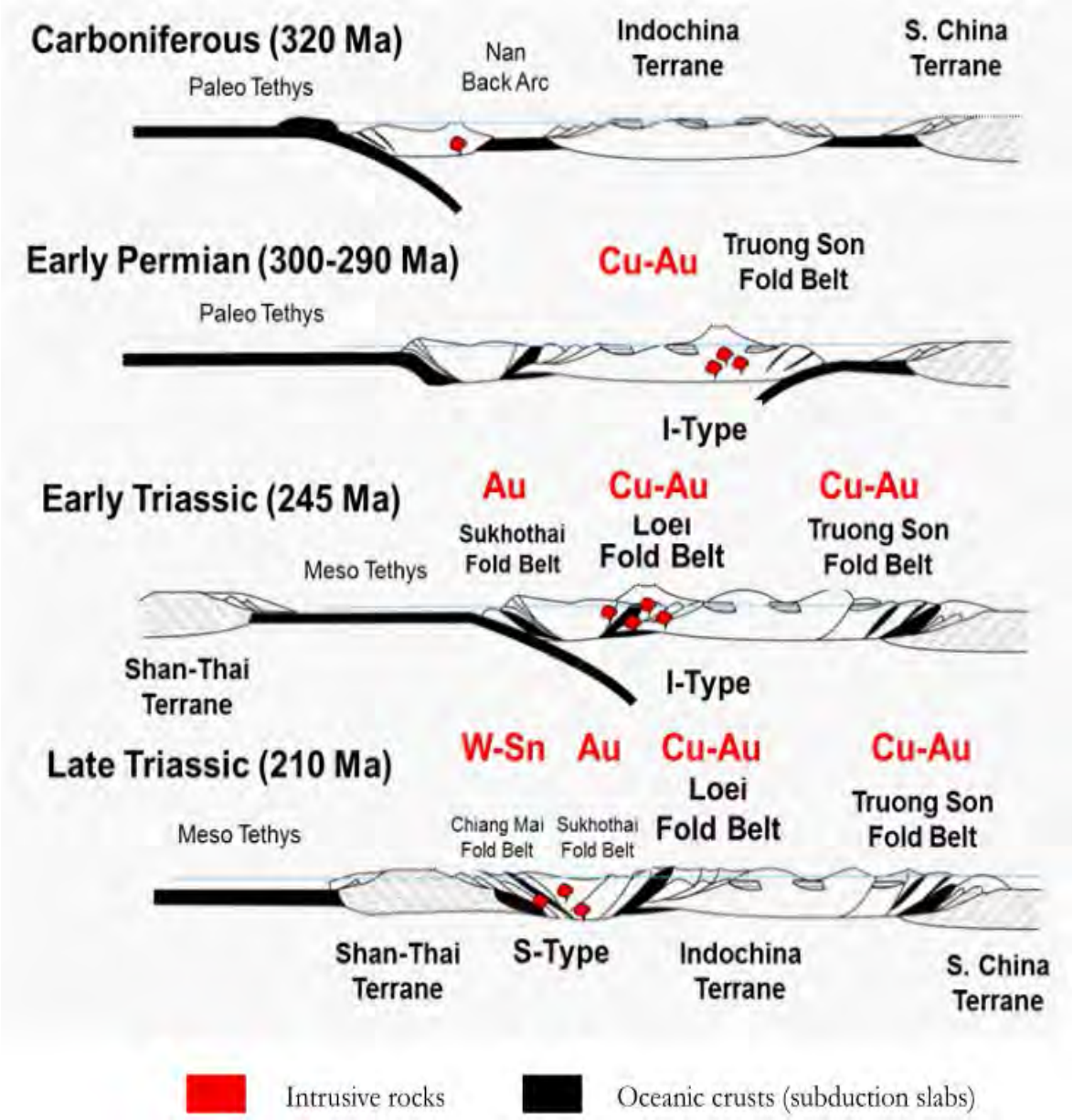

Fig. 2.1 The geotectonic and metallogenic in the age Carboniferous-Triassic (330-210 Ma) showing the association of copper-gold (Cu-Au) with I-type intrusions in Troung Son Fold Belt, the association of gold (Au) in Sukhothai Fold Belt and the association of tungsten-tin (W-Sn) with S-type intrusions (Salam, 2013).

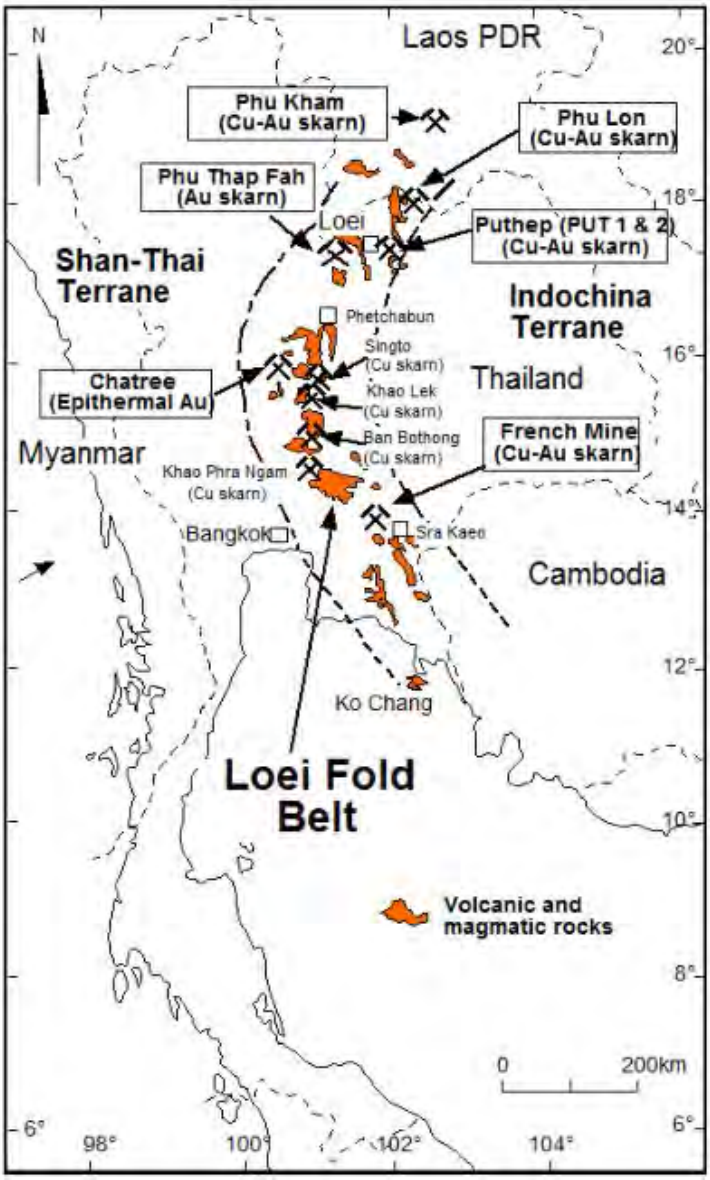

Fig. 2.2 The epithermal and skarn deposits associated along Loei Fold Belt in Laos and Thailand (Salam, 2013).

2.3 LOCAL GEOLOGY

2.3.1 Geology of Phichit Province

Flat plain is the main topographic characteristics in Phichit because of Nan river, Yom river and Phichit river that flow from the north through the south of the province.

Fluvial sediments are deposited widely along the rivers and flood plain. In the eastern Phichit is rolling plain caused by weathering and erosion. The Department of Mineral Resources (DMR, 2007) suggested that the ages of rock basement vary from 286 Ma (mega-annum or a million years).

2.3.1.1 Igneous rock

Igneous rock in Phichit province can be divided by rock type and age range into two rock units: Triassic Khao Rup Chang Granite (Tr_{gr}) and undifferentiated volcanic rock (PT_{Rv}) (DMR, 2007)

Triassic Khao Rup Chang Granite (Trgr) consists of white, light gray to pinkish gray fine-to-medium-grained granite and granodiorite with granular texture comprising mainly of quartz, feldspar, and biotite. This granite rock is distributed as natural outcrops near Nan river.

Undifferentiated volcanic rock consists of rhyolite, andesite, dacite, and basaltic andesite which are distributed as small hills in eastern Phichit such as Khao Phanom Pha, Khao Mo, Khao Tha Phan Nak, Khao, Ched Luk, Khao Pong, and Khao Sai. Khao Mo and Khao Phanom Pha are high-potential for gold mineralization (Fig. 2.3) (Salam, 2013).

2.3.1.2 Sedimentary rock and sediments

Permian Khao Khad Formation (P_{kd}) is the only sedimentary rock found in the Phichit province (DMR, 2007). Quaternary sediments covering of the province are divided into eight sedimentary units which are not described in this chapter.

Khao Khad Formation consists of black to dark grey limestone, chert nodule, dolomite and intercalated with shale, sandstone, tuffaceous sandstone and volcanic rock. The limestone has the presence of fossils: fusulinids, corals,

crinoids, brachiopods, and algae. Khao Khad Formation is distributed in southwestern Wang Sai Phun district.

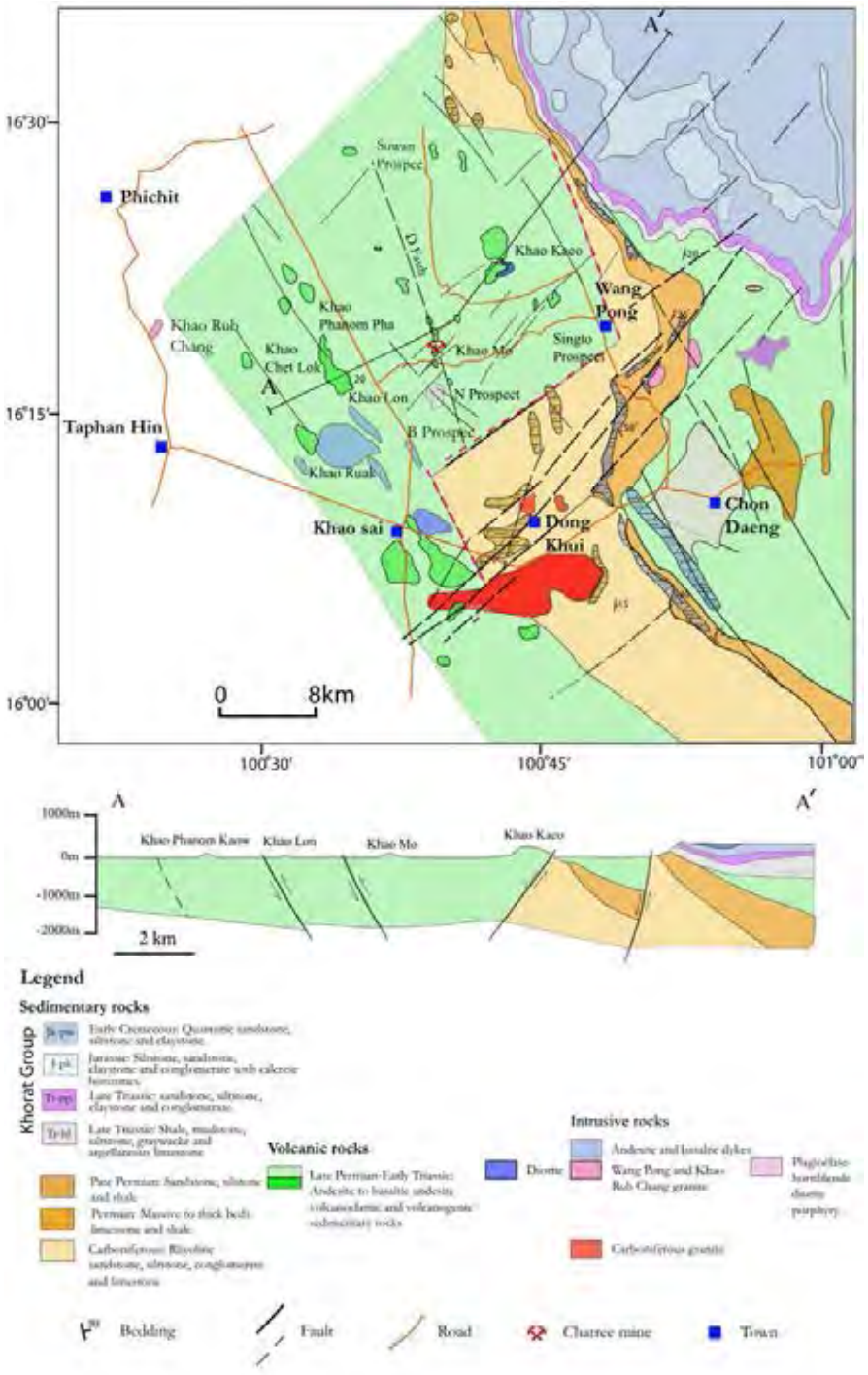

Fig. 2.3 Geological map of the Chatree gold deposit compiled base on map scale 1:250,000 (Salam, 2013).

2.3.2 Geology of Phetchabun Province

Literature reviews for Phetchabun province is only reviewed for rock units near Chatree gold deposit. So, this study focuses on rock units in Wang Pong and Chon Dan districts, Phetchabun province. Phetchabun is located at the edge of Khorat plateau considered various geological characteristics with the age of Carboniferous to Quaternary (DMR, 2008).

2.3.2.1 Igneous rock

Igneous rock in Phetchabun province can be divided by rock type and age ranges into four rock units: Permian volcanic rocks (245-286 Ma), Permo-Triassic volcanic rock (210-286 Ma), Triassic plutonic rock (210-245 Ma), and Tertiary volcanic rock (1.6-66.4 Ma).

Permian volcanic rocks consist of grayish green polycrystalline andesite and light gray polycrystalline rhyolite. The andesite contains porphyry hornblende and the rhyolite contains plagioclase and quartz phenocrysts. Permo-Triassic volcanic rocks mainly consist of rhyolite associated with basaltic andesite, tuff and welded tuff. This rock unit is occurred as dikes, sills, lava flow, and pyroclastic deposits. Rhyolite is monocrystalline but andesite is polycrystalline with hornblende, clinopyroxene and plagioclase phenocrysts. This rock unit is present in all over Phetchabun, especially in northern, central and western of the province. The Triassic plutonic rocks consist of biotite granite, biotite-muscovite granite, and tourmaline granite which are distributed in central and western Phetchabun. Polycrystalline texture of these granites is present with hornblende, tourmaline, and feldspar phenocrysts. Tertiary volcanic rocks mainly consist of dark gray to black basalt which textures vary from dense to vesicular. Olivine and pyroxene phenocrysts are present in the rock. However, southern Phetchabun areas have

more abundance of grayish red rhyolite and greyish green andesite with aphanitic texture.

2.3.2.2 Sedimentary rock and sediments

Carboniferous rock (286-360 Ma) in Phetchabun is Wang Sa Phun Formation which comprises gray metashale, brown to brownish grey shale, gray chert, brown sandstone and conglomerate. This formation is distributed as natural outcrops in Chon dan district located in western Phetchabun.

Carboniferous to Permian rocks (245-360 Ma) are located next to Carboniferous rock comprising black to greenish gray sandstone, siltstone, shale, and mudstone. Conglomeratic rock and metashale are exposed in some areas. Carboniferous to Permian rock is present in Wang Pong, Chon Dan, and Wichian Buri districts located in western Phetchabun.

Permian rocks (245-286 Ma) consist of Tak Fa Formation, Pha Nok Khao Formation, Hua Na Kham Formation, and Nam Duk Formation. Tak Fa Formation comprises gray to black limestone containing black chert nodule and gray shale which is distributed in central and western Phetchabun. Pha Nok Khao Formation comprises gray limestone, gray and yellowish-brown shale and gray chert which is present from Chon Dan to Nhong Phai districts. Hua Na Kham Formation comprises clastic sedimentary rock: yellow sandstone, gray shale, siltstone, and limestone lens. The volcanic rocks: pyroclastic volcanic rock, andesite, tuff, and agglomerate are exposed in some areas. This formation is distributed from eastern to southern Phetchabun Province. Nam Duk Formation comprises blackish gray/reddish brown shale, limestone lens, yellowish/reddish brown sandstone with cross-bedding structure and siliceous cementation. This formation is exposed from northern to southern Phetchabun.

2.3.3 Geology of Chatree Gold Deposit

The Chatree gold deposit is located in Loei Fold Belt associated with Permo-Triassic volcanic rock and volcaniclastic rock. Salam (2013) made a geological mapping that shows geological rock units and stratigraphy of Chatree gold deposit: fiamme breccia unit, volcanogenic sedimentary unit, polymetric mafic intermediate-mafic breccia unit and porphyritic andesite unit in Figure 2.4. The geological map also shows two main fault directions: NNW-SSE and NE-SW, considered an important geological structure that leads to gold mineralization when faults are crossed.

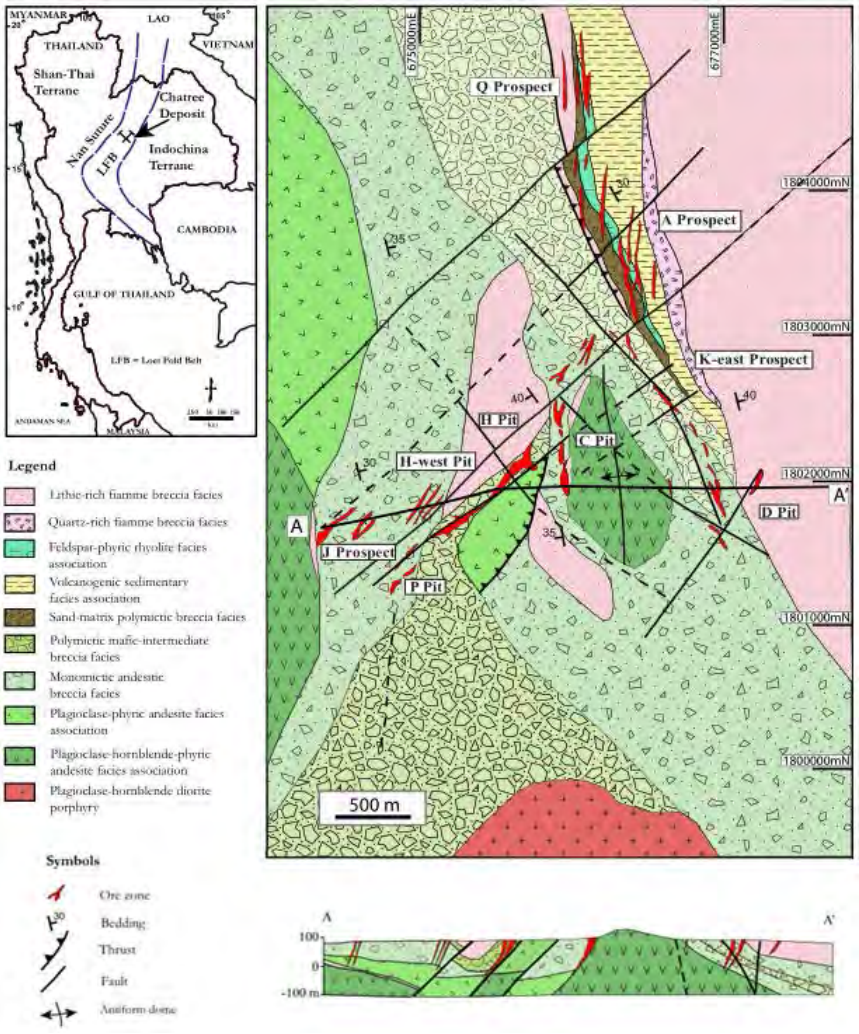

Fig. 2.4 Geological map of Chatree gold deposit after Salam, 2013.

CHAPTER III

METHODOLOGY

3.1 INTRODUCTION

There are two parts in this chapter: Alteration mapping, and field study and sampling. The first part comprises acquired satellite images and transformation; the second part shows the procedure for ground follow-ups. This chapter describes the procedure of this study with a schematic workflow diagram shown in Figure 3.1, modified from Zhang et al. (2007; Fig. 3.2).

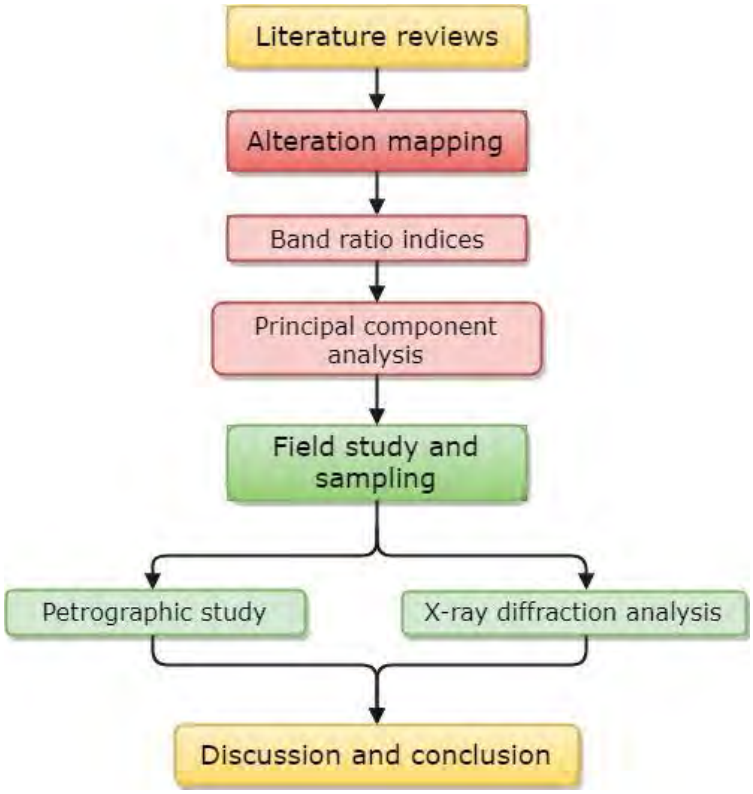

Fig. 3.1 Schematic diagram showing sequences of this research.

3.2 ALTERATION MAPPING

The ASTER Level-1B satellite images are acquired on January 5, 2001, before the initial mining operation. The Level-1B data contain radiometrically calibrated and geometrically co-registered data for preprocessing considered essential for atmospheric corrections (Ninomiya, 2003). ASTER bands 4-9 with an image spatial resolution of 30x30 square meters were chosen for the reflectance and absorption features or spectral signatures of individual alteration minerals in SWIR wavelength, which was resampled at the ASTER bands using data from spectral library of The United States Geological Survey (USGS) (Fig. 3.3). According to illite abundance at Chatree gold deposit (Lunwongsa et al., 2011), the USGS illite spectral signature from USGS in Figure 3.3A is compared to the Chatree illite spectral signature (Fig. 3.4); The highest and lowest reflectance for illite in SWIR is about 1700 and 2200 μm, respectively, which are resampled at bands 4 and 5 jointly. However, the band ratio indices from Fatima et al., 2017 are not able to detect high-potential gold mineralization areas at Chatree gold deposit because of specific mineral indices and vegetation covering. So, the OH-bearing altered minerals index (OHI) proposed by Ninomiya (2003) was used to detect a group of hydroxyl-group bearing alteration minerals instead.

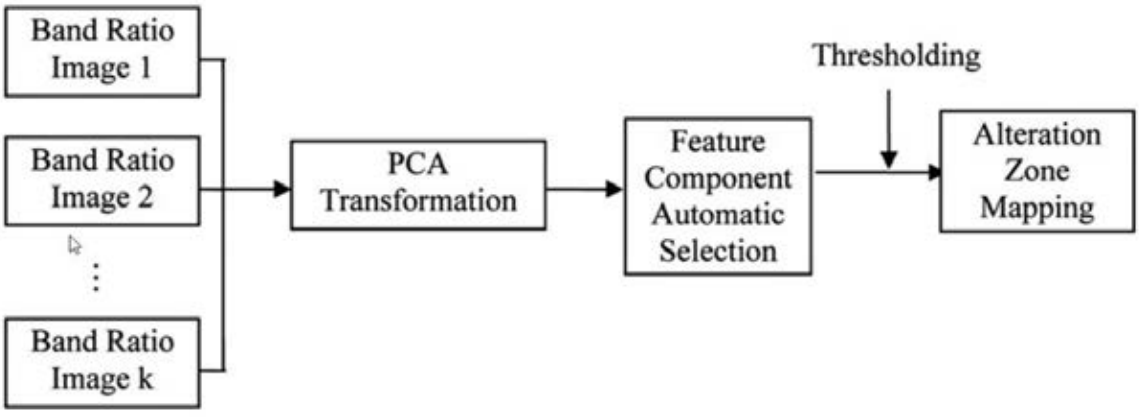

Fig. 3.2 Flowchart for PCA transformed indices approach (Zhang et al., 2007).

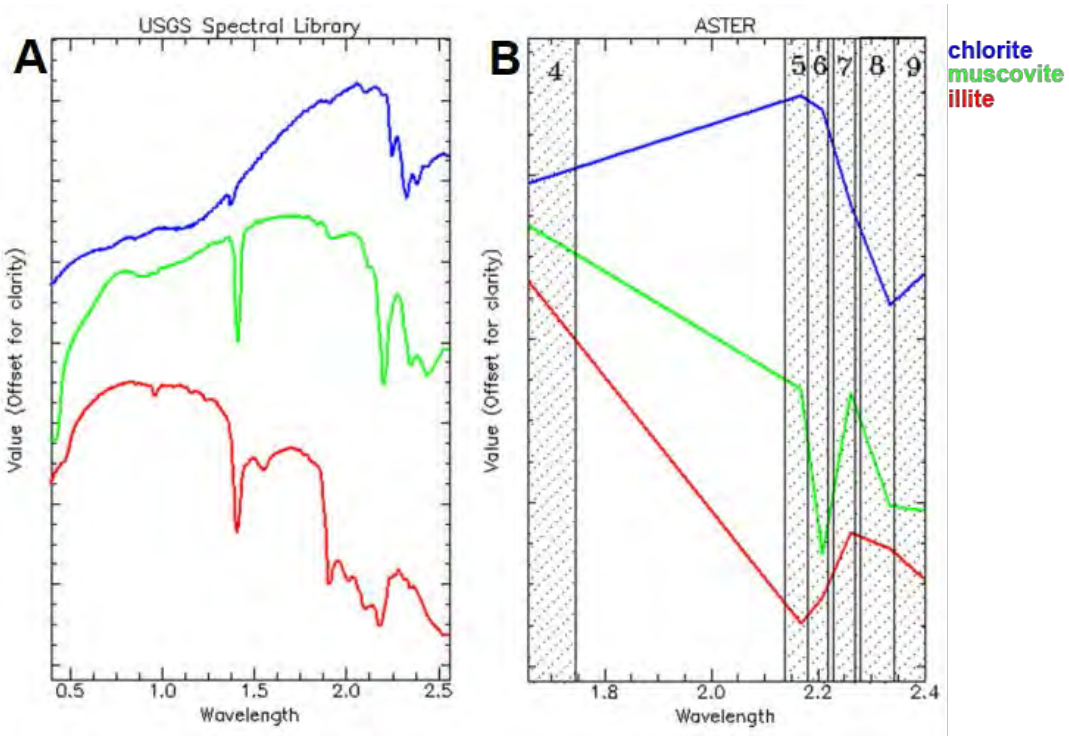

Fig. 3.3 Spectral signatures of chlorite, muscovite and illite **A.** USGS spectral library, **B.** resampled at ASTER bands. (Fatima et al., 2017).

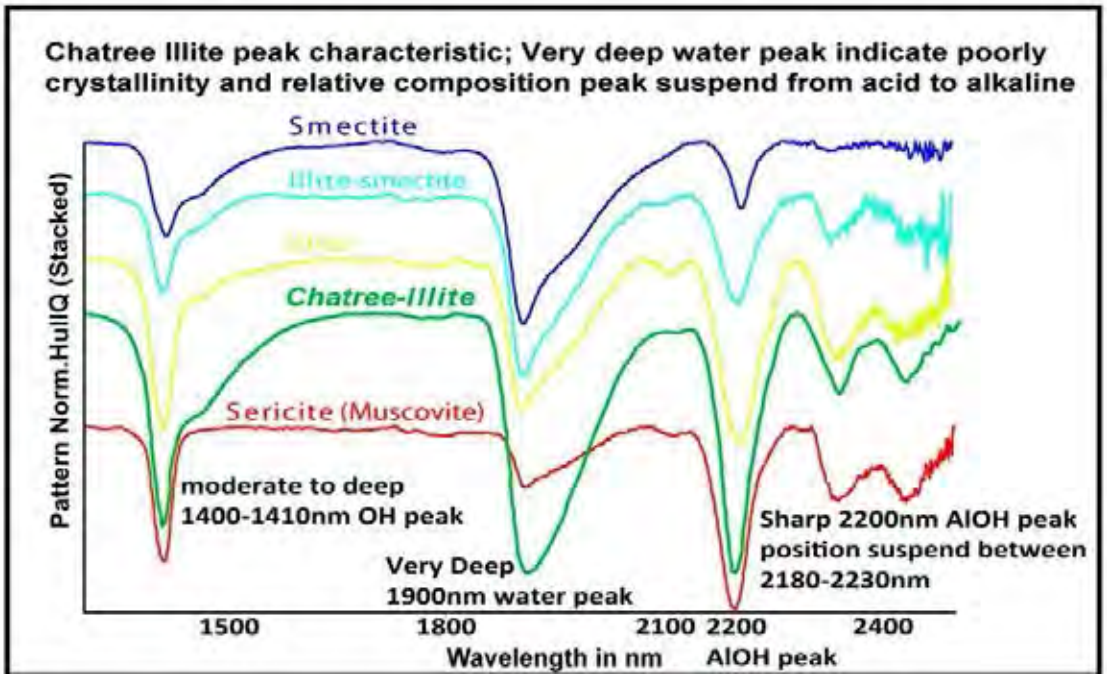

Fig. 3.4 Chatree illite characteristic peak using Analytical Spectra Devices (ASD) (Lunwongsa et al., 2011).

3.2.1 BAND RATIO

One vegetation index and three mineral indices in Table 3.1 are defined from the spectral reflectance characteristics of the target objects using Esri ArcMap software on ASTER satellite images covering the study area. The stabilized vegetation index (StVI) was used to detect the vegetation against seasonal change of radiance from the atmosphere which is selected for one of the principal components (PC) in PCA. OH-bearing altered minerals index (OHI) was selected to detect the OH-bearing altered minerals on the surface formed by hydrothermal alteration. The kaolinite index was used to detect kaolin group of clay minerals which is not associated in low-sulfidation deposit due to less acidic conditions. The calcite index (CLI) is used to indicate hydrothermal veins in the epithermal deposit. The mineral indices: OHI, KLI and CLI are composed in a band composition image (RGB) respectively, for the first alteration map. Alteration minerals mineralized in low-sulfidation epithermal environments are shown in pink because of high detection from OHI in the red band and CLI the blue band (Fig. 4.1).

Table 3.1 Mineral indices used for alteration mapping (Ninomiya, 2003).

Index names	Band ratio indices
Stabilized vegetation index (StVI)	$\frac{Band3}{Band2} * \frac{Band1}{Band2}$
OH-bearing altered minerals index (OHI)	$\frac{Band7}{Band6} * \frac{Band4}{Band6}$
Kaolinite index (KLI)	$\frac{Band4}{Band5} * \frac{Band8}{Band6}$
Calcite index (CLI)	$\frac{Band6}{Band8} * \frac{Band9}{Band8}$

3.2.2 PRINCIPAL COMPONENT ANALYSIS

The band ratio index can be contaminated with unwanted materials that have similar reflectance features to target objects. So, PCA is used in this study using Esri ArcMap software to select a principal component which has smaller variances. The band ratio indices: StVI, OHI, KLI and CLI were chosen to apply PCA transformation. The eigenvector values in Table 3.1 are transformed into four principal component analysis images shown in Figure 3.2 where higher eigenvectors are brighter pixels and lower eigenvectors have darker pixels. The criteria for selecting a proper principal component is the target object's eigenvector values and the unwanted values from the other PCs. The most suitable principal component for this study is PC2, because the highest eigenvectors are 0.80689 for the input band OHI and the lowest eigenvectors are -0.39145 and -0.34326 respectively for the input bands CLI and StVI as unwanted materials. However, PC2 is slightly affected when detecting OH-bearing altered minerals from the input band KLI which has positive eigenvectors (0.25001). The PC2 image is reclassified with 1% highest DN value for high-potential gold mineralization map using ENVI software (Geoimage, 2005). The high-potential gold mineralization map in Figure 4.2 is used for selecting representative areas to collect surficial rock samples that may provide reflectance from OH-bearing altered minerals.

Table 3.2 Principal component analysis on band ratio indices of ASTER satellite images with selected spatial mineral index scenes calculating for eigenvectors and eigenvalues.

Input band ratio indices	StVI (B3/B2)*(B1/B2)	OHI (B7/B6)*(B4/B6)	KLI (B4/B5)*(B8/B6)	CLI (B6/B8)*(B9/B8)	Eigenvalues (%)
PC1	0.91137	0.36495	-0.22707	-0.00292	74.2546
PC2	-0.34326	0.80689	0.25001	-0.39145	19.9675
PC3	-0.22707	0.47979	-0.53469	0.69386	4.3676
PC4	-0.00292	-0.02987	0.77463	0.60442	1.4103

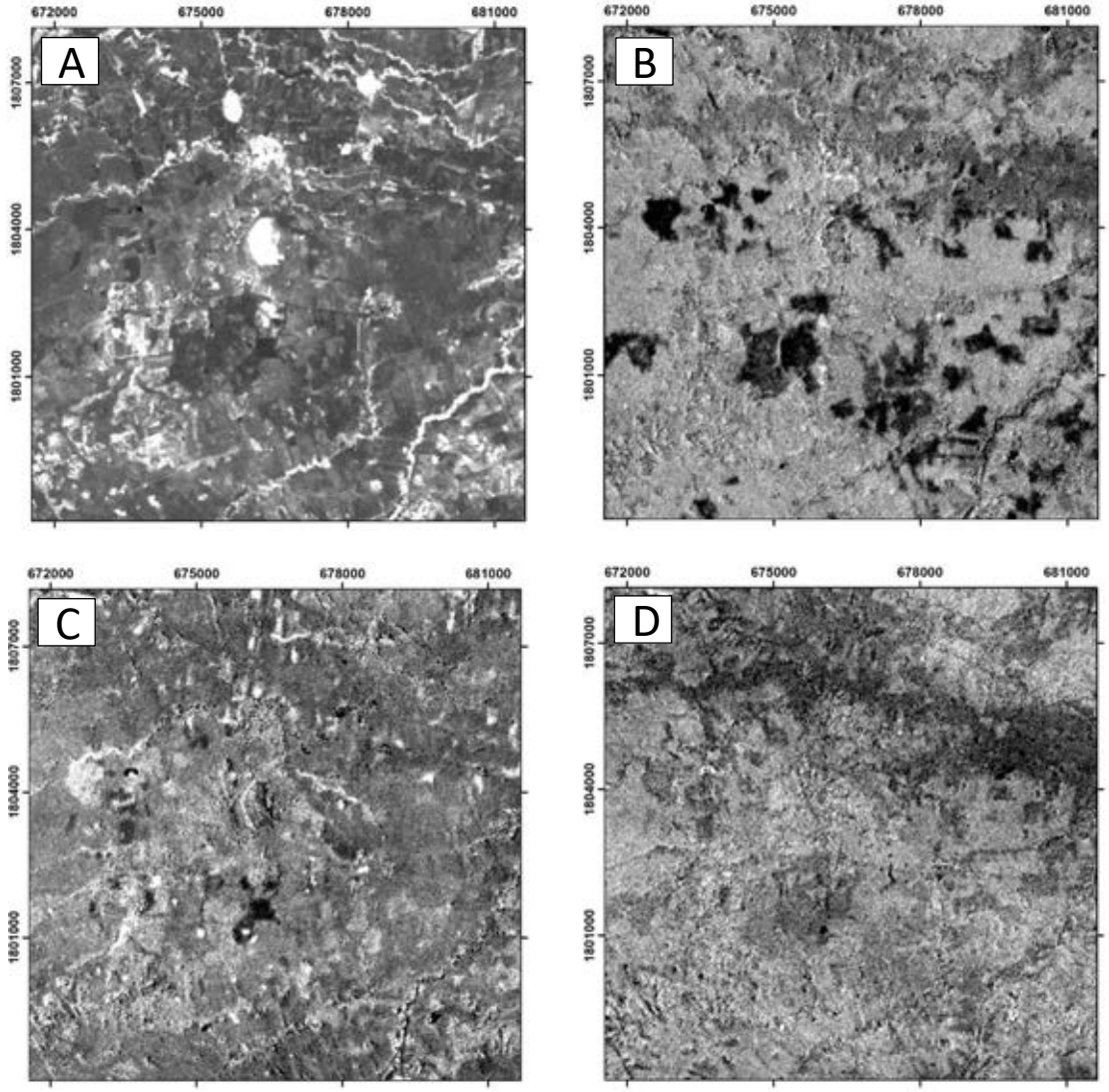

Fig. 3.5 Images of four principal components: **A.** PC1, **B.** PC2, **C.** PC3 and **D**. PC4 from eigenvectors on Table 4.1.

3.3 FIELD STUDY AND ROCK SAMPLING

Rock samples were collected on November 8 - 11, 2017 from four representative areas near Chatree pit limits which are not disturbed by humans' activities such as mining, agriculture and or waste disposal. This study is based on The World Geodetic System 1984 (WGS84) datum with Universal Transverse Mercator (UTM) system in the 47Q zone which

is mainly located in northern Thailand (Table 3.3). The easting (horizontal axis) and northing (vertical axis) coordinates are recorded in meters.

The Amphoe Wang Sai Phoon 1:50,000-scale topographic map of the study area in the series L7018 and the position 5141 IV is derived from the Royal Thai Survey Department (RTSD) (Fig. 3.6). This topographic map is used to compare to the high-potential gold mineralization map (Fig. 4.2) and select sampling locations in undisturbed areas.

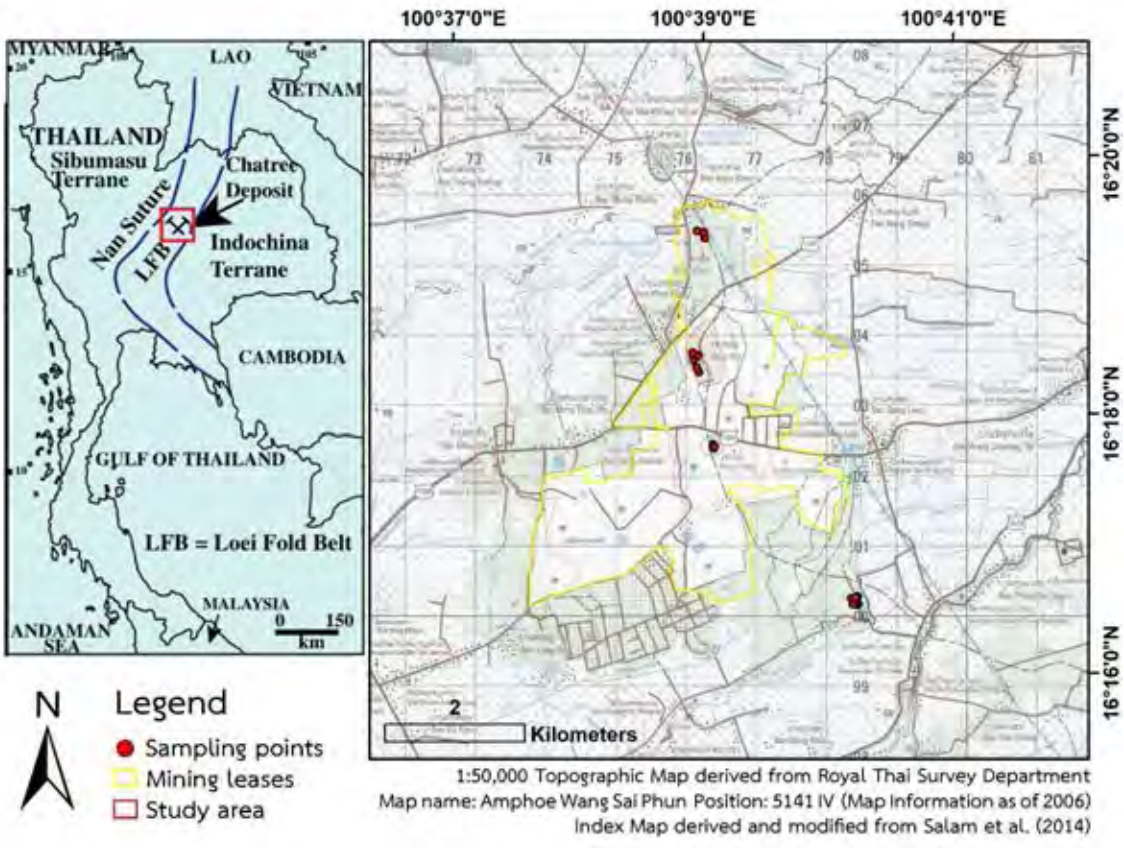

Fig. 3.6 The study area located in Loei Fold Belt shows sampling points and mining leases on topographic map.

The sampling locations: Q pit, Khao Mo, Khao Pong, and B prospect were chosen based on the high-potential gold mineralization map in Figure 4.2 and the Chatree

prospect areas that were already surveyed. The sampling locations are located in highlands considered highly resistant due to silicification by hydrothermal quartz veins in epithermal environments. The selected sampling areas are covered with vegetation, especially

B prospect and Khao Pong (Figs. 3.7A, 3.7B). Khao Mo and Q pit areas may correspond to the detection of OH-bearing altered minerals because of exposed soil and rock (Fig. 3.7C, 3.7D). The rock samples collected on the surface are hard due to silicification which can preserve clay minerals considered easily weathered.

Fig. 3.7 Sampling areas: **A.** B prospect, **B.** Khao Mo, **C.** Khao Pong, and **D.** Q pit.

Table 3.3 Rock sampling and analysis methods.

No.	Sample no.	Description	EASTING	NORTHING	Thin section	XRD analysis
1	B01	Float rock on the hill	678352	1800256		✓
2	B08	Float rock on the hill	678377	1800172	✓	✓
3	B09	Float rock on the hill	678442	1800284	✓	
4	B010	Float rock on the hill	678420	1800271		✓
5	KM01	Float rock on the hill	676179	1803469		✓
6	KM02	Float rock on the hill	676147	1803534	✓	✓
7	KM03	Float rock on the hill	676106	1803650	✓	✓
8	KP01	Float rock on the hill	676383	1802453	✓	✓
9	KP02	Float rock on the hill	676381	1802410	✓	✓
10	KP03	Float rock on the hill	676391	1802411		✓
11	KP04	Outcrop	676390	1802394	✓	
12	Q01	Float rock on the hill	676263	1805385	✓	✓
13	Q02	Float rock on the hill	676253	1805460		✓
14	Q03	Float rock on the hill	676154	1805482	✓	✓

3.4 PETROGRAPHIC STUDY

The rock samples B08, B09, KM02, KM03, KP01, KP02, KP06, Q01, and Q03 were selected for petrographic thin-section study due to the consolidation of rock samples (Table 3.3). In the case of volcanic breccia thin sections, melted balsam was put on the target side of rock slab to increase the hardness before polishing (Fig. 3.8). The petrographic

Fig. 3.8 Thin section preparation. **A.** Melted balsam put on the target side of rock slab, **B.** rock slabs.

study for alteration minerals can be difficult to identity due to the extremely fine grain size from recrystallization of primary minerals in low temperature conditions. However, illite-sericite, microcrystalline quartz, hornblende, chlorite, and K-feldspar (orthoclase) are identified using plain polarized light (PPL) and cross plain polarized light (XPL) under microscope.

3.5 X-RAY DIFFRACTION ANALYSIS

Mineral identification by petrographic study cannot provide mineral amount. So, x-ray semi-quantitative analysis is used in this study for better comparison with the high-potential gold mineralization map. X-ray diffraction is an instrumental method used to identify minerals by the diffraction of x-ray beams.

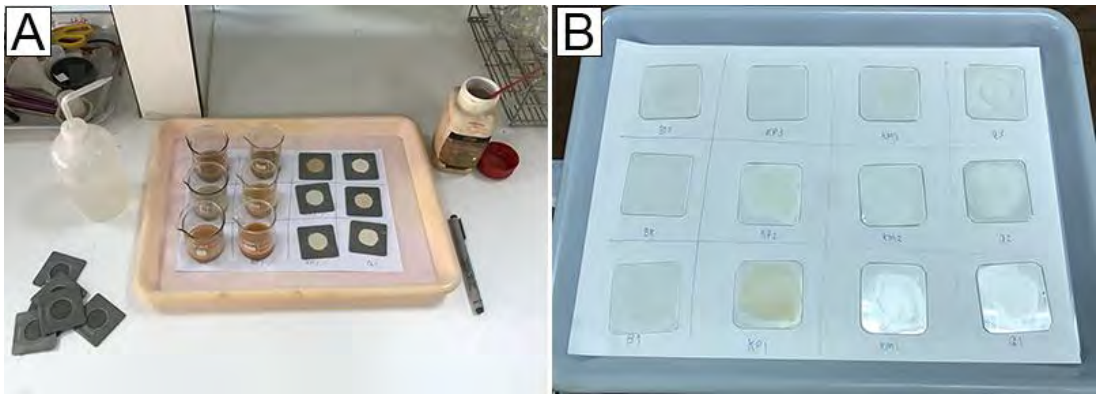

Fig. 3.9 Orientated powder samples preparation. **A.** Sodium hexametaphosphate used for quartz precipitation, **B.** Dry powder samples on glass plates.

The rock samples B01, B08, B10, KM01, KM02, KM03, KP01, KP02, KP03, Q01, Q02, and Q03 were selected for powder specimens using a rock grinding machine. The orientation for clay minerals is applied to reduce quartz amount in the powder samples that can interfere with the detection of other minerals. Sodium hexametaphosphate ($(NaPO_3)_6$) is used with each powder sample by mixing with distilled water in a beaker and leaving overnight (Fig. 3.9A). Subsequently, the liquid in each beaker was stirred gently and

dropped on a glass plate leaving until it dries out (Fig. 3.9B). The twelve dry powder samples were analyzed for x-ray diffraction patterns by an x-ray diffractor in the laboratory (the Department of Geology, Faculty of Science, Chulalongkorn University) The diffraction started from 5° to 30° with an increment of 0.02° and the scan speed at 1 sec/step (the condition and specification of the x-ray diffractor are given in Appendix B).

CHAPTER IV

RESULTS AND INTERPRETATION

4.1 INTRODUCTION

The results of this study are divided into two parts. The first part is the high-potential gold mineralization map which was processed with two image transformations: band ratio and principal component analysis. The second part is the ground follow-ups: petrographic study and x-ray diffraction analysis.

4.2 SATELLITE IMAGE TRANSFORMATION

4.2.1 BAND RATIO

The band ratio indices called mineral indices (Ninomiya, 2003) are applied to the ASTER satellite images. The band composition with indices: OHI, KLI and CLI in RGB respectively is created for alteration mapping (Fig. 4.1). This map shows high detection of OH-bearing altered minerals and calcite which are the associated alteration minerals in epithermal system in pink (Salam, 2013). The green area shows higher detection of kaolinite than the other alteration minerals from input indices. The green area is detected for kaolin group of minerals which can be contaminated with similar spectral signatures.

4.2.2 PRINCIPAL COMPONENT ANALYSIS

The ASTER mineral index images from band ratio transformation are applied with principal component analysis. Four principal component analysis images are shown in Figure 3.2. The first principal component (PC1) accounts for 74.2546% of the total eigenvalues and is composed of a positive weighting from bands StVI and OHI which are considered most of the spectral data in the scene (Jensen, 2005). This principal component shows the highest eigenvectors of vegetation variations (0.91137) which is statistically prominent because StVI (Table 3.2) is unable to distinguish vegetation and OH-

bearing altered minerals. The PC2 shows the highest eigenvectors on OHI band (0.80689) shown as bright pixels which is the desired principal component for high-potential gold mineralization map due to the limited potential for vegetation disturbance (-0.34326). The eigenvector values for kaolinite and calcite are 0.25001 and -0.39145 respectively. So, the KLI contribution can slightly affect to the detection of OHI due to the hydroxyl group in kaolinite composition which the calcite contribution using CLI is the lowest. The PC2 is then reclassified with 1% highest DN values in the image for high-potential gold mineralization areas (Fig. 4.2). The PC3 is good for calcite detection in bright pixels with 0.69386 of eigenvectors. The PC4 is the combination of calcite and kaolinite detection due to higher eigenvectors (0.77463 and 0.60442 respectively).

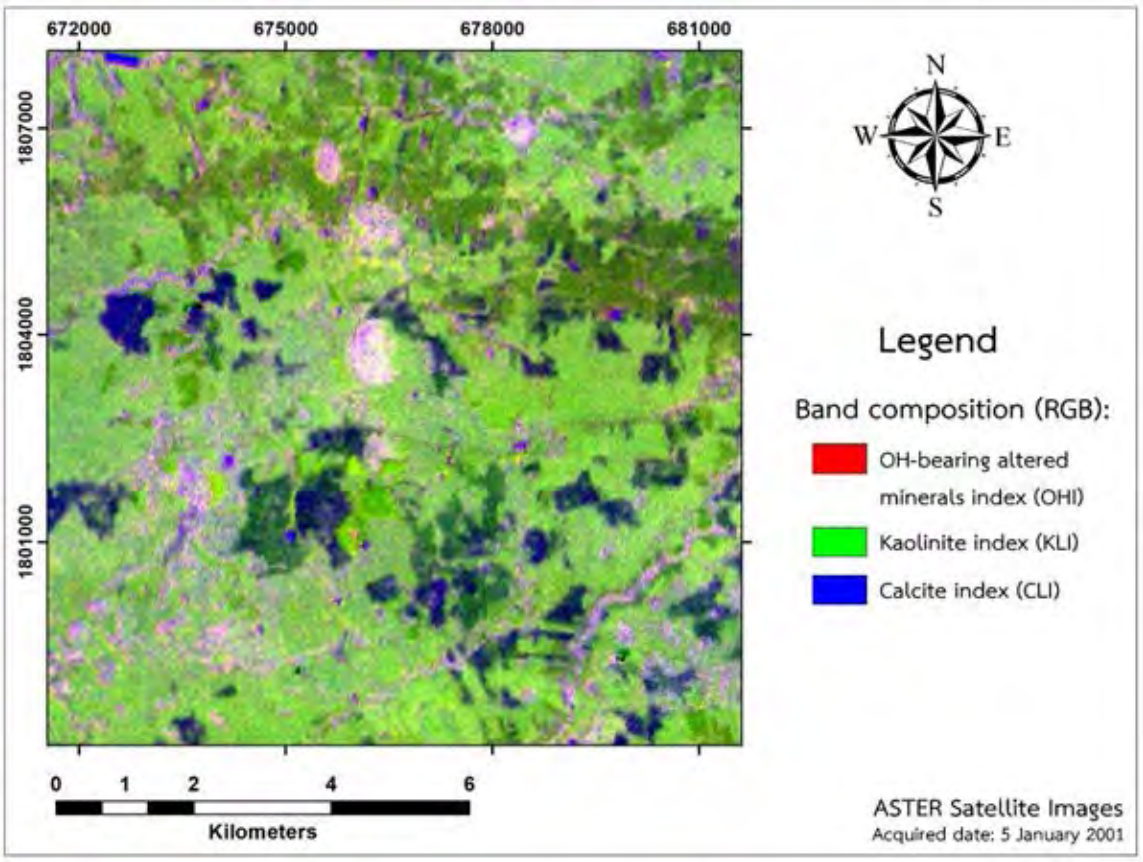

Fig. 4.1 Image of ASTER band ratio indices: OHI, KLI and CLI in RGB showing the alteration zones in pink.

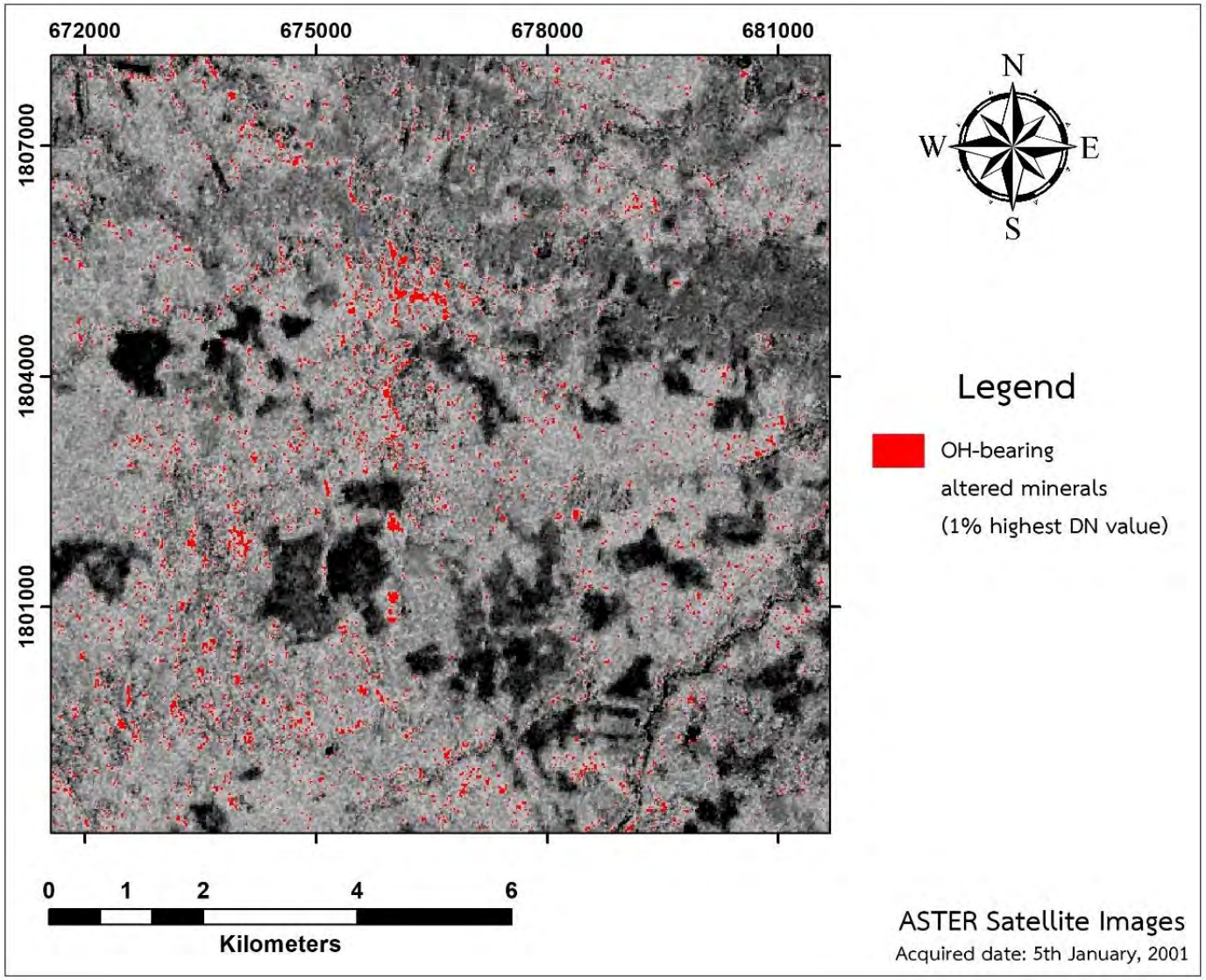

Fig. 4.2 High-potential gold mineralization map from the PC2 with 1% highest DN value showing the OH-bearing altered mineral detection in red.

4.3 PETROGRAPHIC STUDY

Volcanic breccia is white to reddish white (color on fresh surface) and brown (color on weathered surface) which is widely distributed from representative locations. Quartz mineralization is common in open space or vug with the length 1/2 to 1 cm (4.4A). The size of volcanic clasts varies from 1/4 to 1 cm which is hard to define due to alteration of rock (4.5A). Most of the samples are float rocks collected from undisturbed areas (in situ) in the hills and highlands.

Plagioclase-hornblende phyric andesite is collected from Khao Pong which is considered to be natural outcrop and slightly weathered. The andesite is dark green (color on fresh surface) and brown (color on weathered surface) in hand specimen with plagioclase and hornblende phenocrysts which are 1/8 to 1/2 in grain size (Fig. 4.5A). The plagioclase grain is white to brown and the hornblende grain is black in color.

Thin-section samples from four different areas show the characteristics of argillic alteration which is present with the mineralogy: quartz, illite, sericite, adularia, chlorite, and calcite. Argillic alteration is known as an extensively distributed alteration type at Chatree gold deposit (Salam, 2013). Illite-sericite is the most common mineral in this alteration found as the replacement of k-feldspar in breccia grains (Figs. 4.4B, 4.4C). Open space in the country rock can be filled with newly precipitated mineral from hydrothermal fluids such as microcrystalline quartz and adularia and adularia subsequently altered to illite-sericite (Figs. 4.3B, 4.3C). Adularia is the temperature indicator in epithermal environment associated with microcrystalline quartz (Salam, 2013) (Figs. 4.3D, 4.3E). One common argillic characteristic is the alteration of hornblende to chlorite associated with microcrystalline quartz (Fig. 4.5).

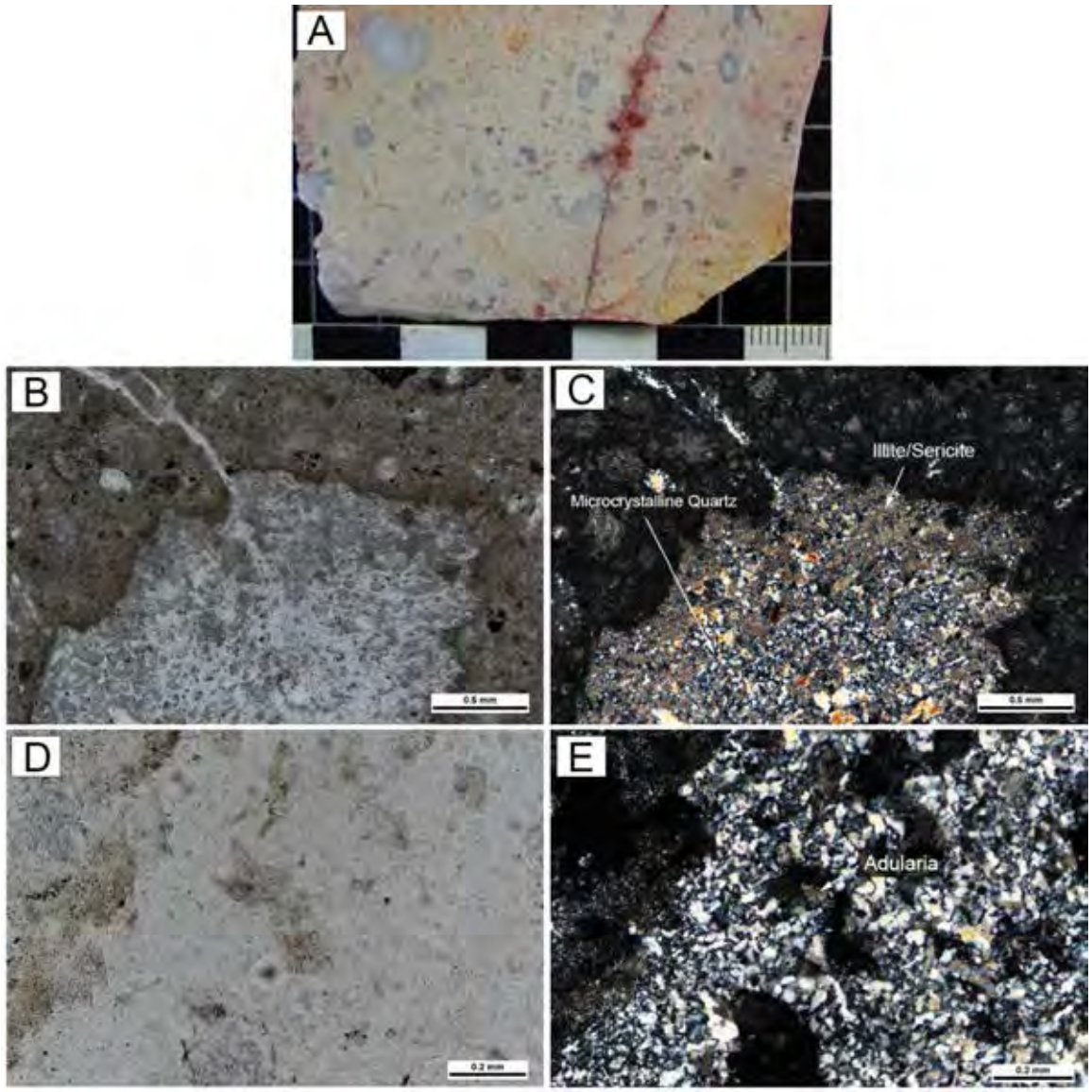

Fig. 4.3 Characteristics of open space filling fracture and vug and hydrothermal alteration. **A.** Photograph of rock slab showing relic of volcanic breccia (white rock fragments), **B.** Photomicrograph showing hydrothermal infill (PPL), **C**. Photomicrograph showing illite-sericite associated with microcrystalline quartz in the open space (XPL), **D.** Photomicrograph showing adularia in rhombohedral shape (PPL), **E.** Photomicrograph showing adularia associated with microcrystalline quartz (XPL). Sample B08 taken from B prospect.

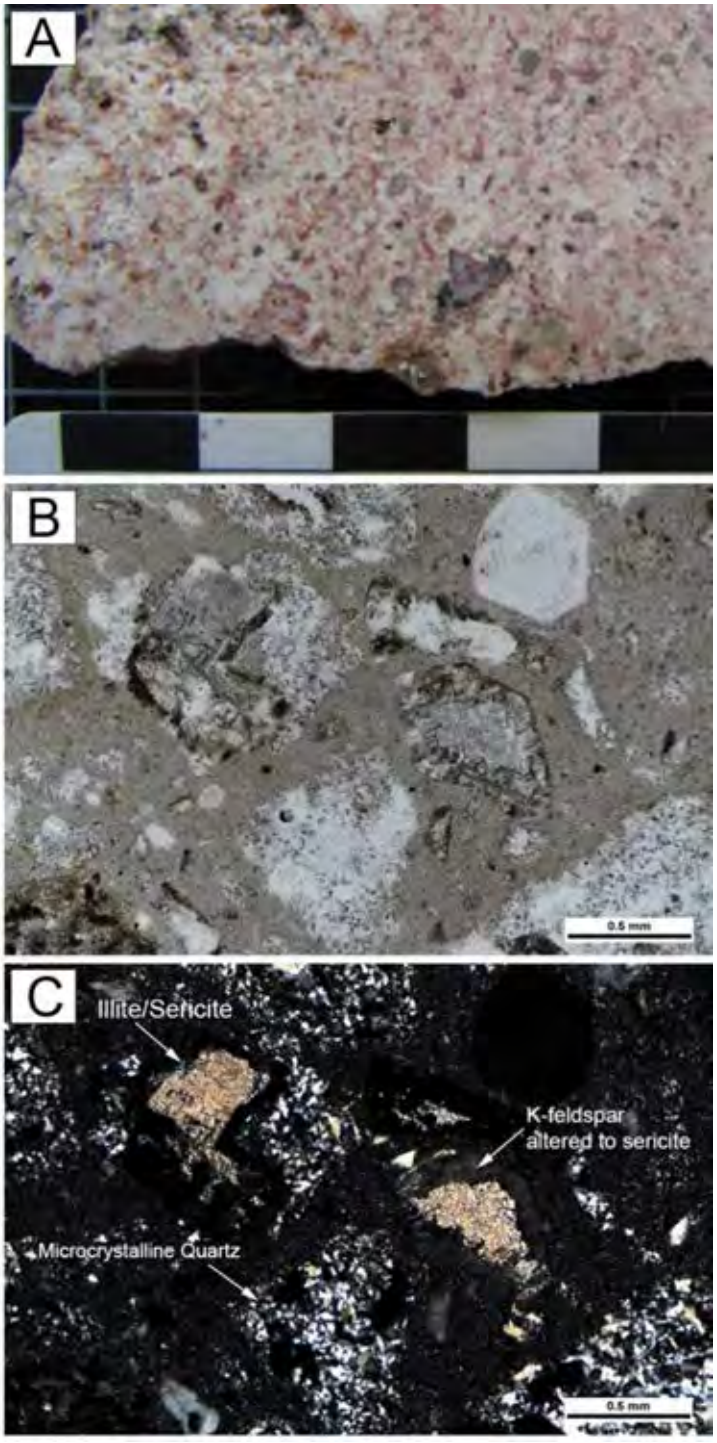

Fig. 4.4 Characteristics of altered volcanic breccia. **A.** Photograph of rock slab, **B.** Photomicrograph showing altered phenocrysts (PPL), **C**. Photomicrograph showing K-feldspar phenocrysts altered to sericite associated with microcrystalline quartz (XPL). Sample Q03 taken from Q pit.

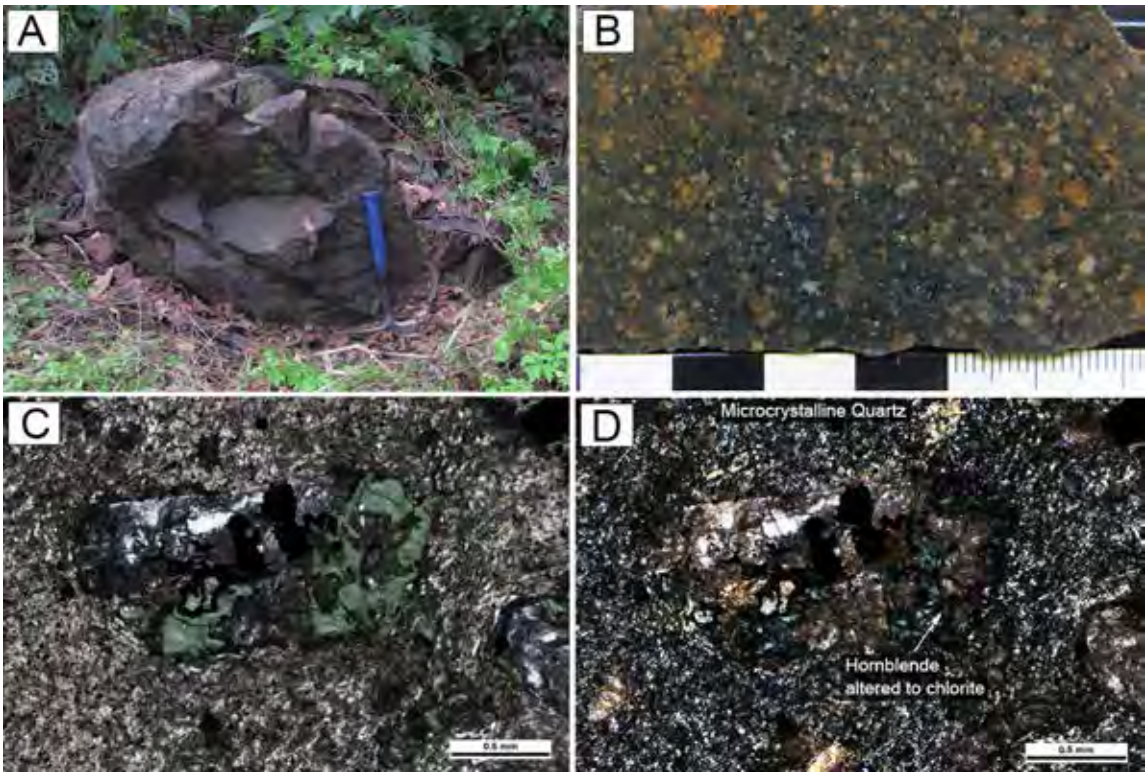

Fig. 4.5 Characteristics of hydrothermally altered plagioclase-hornblende phyric andesite. **A.** Photograph of andesite outcrop found on the top of Khao Pong, **B.** Photograph of rock slab, **C.** Photomicrograph showing altered hornblende phenocryst (middle) (PPL), **D**. Photomicrograph showing hornblende phenocryst altered to chlorite (middle) associated with microcrystalline quartz in the matrix (XPL). Sample KP03 taken from Khao Pong.

4.4 MINERAL COMPOSITION

The twelve oriented powder samples from four sampling locations verify the presence of alteration minerals (Table 4.1). An XRD pattern in Figure 4.6 shows a better detection for mineral identification than the petrographic study, especially alteration minerals (The other XRD patterns are in Appendix B). The XRD patterns are determined for mineral assemblages in the rock samples by using the semi-quantitative XRD analysis (Table 4.1). XRD analysis shows variable amounts of albite (1-30%, avg. 8%), adularia (1-9%, avg. 2%), quartz (26-72%, avg. 52%), illite (2-35%, avg. 17%), sericite (1-27%, avg. 6%), chlorite (2-18%, avg. 4%), calcite (1-10%, avg. 5%), kaolinite (1-19%, avg. 4%),

and montmorillonite (1-27%, avg. 4%). The OH-bearing altered minerals: illite, sericite, chlorite, kaolinite and montmorillonite are consistent with the high-potential gold mineralization map (Fig. 4.2).

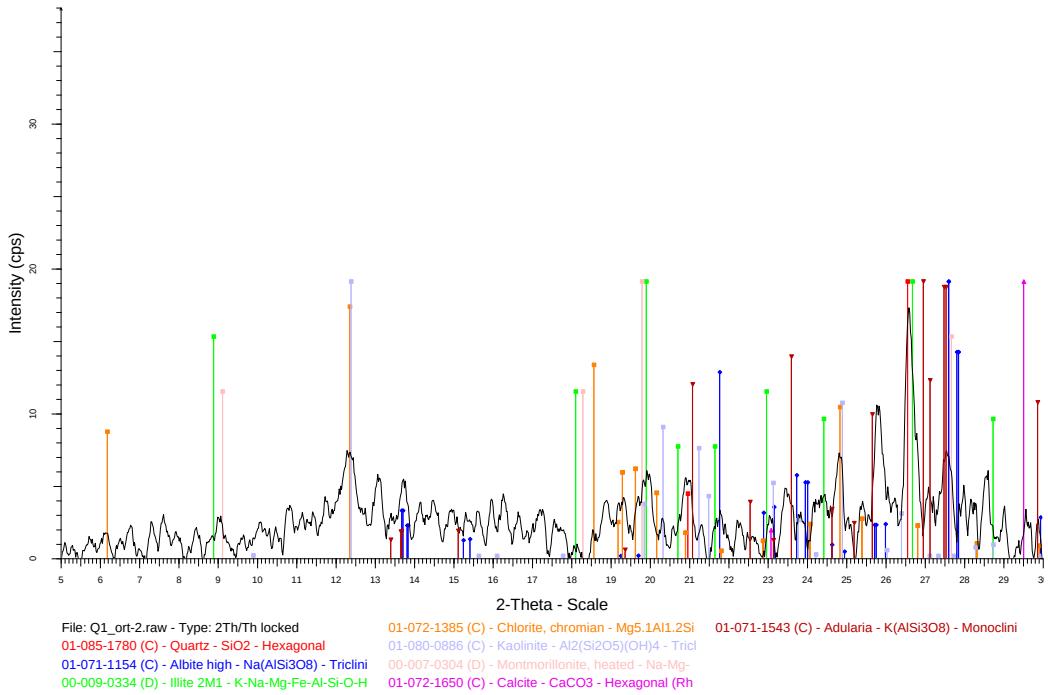

Fig. 4.6 X-ray diffraction pattern showing the diffraction peaks for detected minerals. Scale is in 2-Theta (degrees) and counts per second (CPS) for the intensity. Sample Q01 taken from Q pit.

Table 4.1 XRD result from selected rock samples.

Sample No		XRD semi-quantitative analysis								
		Albite (%)	Adl (%)	Qtz (%)	Illite (%)	Sericite (%)	Chl (%)	Calcite (%)	Kaol (%)	Mont (%)
B-prospect	B01	4.49	0	72.22	21.56	1.72	0	0	0	0
	B08	7.89	7.43	62.39	2.45	12.91	5.19	1.74	0	0
	B10	1.85	0	64.64	28.84	2.84	2.81	1.85	0	0
Khao Pong (C pit footwall)	KP01	15.77	8.66	26.37	22.37	0	18.10	8.73	0	0
	KP02	4.88	0	47.26	16.99	4.14	3.45	4.26	19.03	0
	KP03	30.36	0	42.23	24.51	0.57	0	0	2.33	0
Khao Mo (A pit)	KM01	3.94	1.18	36.16	23.69	20.42	7.38	7.21	0	0
	KM02	5.07	2.67	45.40	34.54	0	4.67	5.95	0	1.70
	KM03	5.44	1.07	51.72	4.10	27.89	0	3.79	0	1.34
Q pit	Q01	10.72	3.73	58.80	4.46	0	3.25	9.04	2.53	7.47
	Q02	3.94	0	54.59	5.73	0	0	8.71	0	27.04
	Q03	7.29	1.07	62.17	15.15	0	0	1.82	6.11	6.39

Abbreviation: Adl = adularia, Qtz = quartz, Chl = chlorite, Kaol = kaolinite and Mont = montmorillonite

CHAPTER V

DISCUSSION AND CONCLUSION

5.1 DISCUSSION

5.1.1 Remote Sensing and Ground Follow-ups

The high-potential gold mineralization areas are successfully mapped for Chatree gold deposit by the detection of OH-bearing altered minerals using the image transformations: band ratio and PCA. The OHI, one of band ratio indices (Ninomiya, 2003), generally varies with the abundance of hydroxyl-bearing altered minerals on the surface which can be sensitive to vegetation and relatively insensitive to variations in lithology (Pour et al., 2013). So, principal components from band ratio indices: StVI, OHI, KLI and CLI can statistically improve the detection of the high-potential mineralization map (Fig. 4.2). The high-potential gold mineralization areas in C-H pit and Q pit limits are detected for the gold mineralization with already productive operations (Fig. 5.1). The C pit is confirmed with massive ore veins that can provide thicker alteration zones than the other Chatree pits and prospects considered stockworks or multiple ore veins (Kromkhun, 2005 and Salam, 2013). Petrographic study and XRD result show the detection of OH-bearing minerals: illite, sericite, chlorite, kaolinite, and montmorillonite from selected rock samples which is consistent to high-potential mineralization areas. Adularia ($KAlSi_3O_8$) considered the key mineral for epithermal deposit, is a polymorph of K-feldspar which is not detected due to the lack of a hydroxyl group in mineral composition.

5.1.2 Alteration Minerals and Zones

The selected rock samples from undisturbed areas (e.g. agriculture and mining) classified as volcanic breccia and plagioclase-hornblende phyric andesite are composed of OH-bearing altered minerals, i.e., illite, sericite, chlorite, adularia, kaolinite, and montmorillonite which is consistent with previous studies of the alteration zones (Lunwongsa et al., 2011 and Salam, 2013) and can be interpreted as argillic zone. Argillic

zone considered the outer zone from the hydrothermal veins; it consists of quartz, adularia, illite, calcite, chlorite and pyrite with minor ankerite, kaolinite, and albite (Salam, 2013) (Fig. 5.2). From this study, illite-sericite, kaolinite, and montmorillonite cannot be distinguished with petrographic study due to extremely fine-grained size.

The alteration of feldspars may give free ions to the alteration minerals such as illite-sericite ($KAl_2(AlSi_3O_{10})(OH)_2$) which is considered extremely fine-grained mica mineralized in low-temperature condition (200-300 °C). Adularia is also an alteration mineral formed by a boiling process in epithermal environment that produces alkaline fluid resulting in deposition of adularia (Salam, 2013). The plagioclase-hornblende phyric andesite considered slightly altered rock, shows more detail for alteration in the petrographic study. There is not only hornblende altered to chlorite but also the feldspar grains altered to illite-sericite by hydrothermal reaction.

5.1.3 Comparison between Band Ratio and PCA techniques

Band ratio is the simplest image transformation to identify objects on the surface. The band ratio indices have been created for satellite images to distinguish materials in specific climates**.** However, this method is still contaminated with unwanted objects which can give reflectance in the wavelength of interest. In contrast, PCA can help correlate for each group of the information and principal components show a better separation for the object of interest. So, the combination of band ratio indices and PCA can help improve the individual surficial detection.

5.1.4 Comparison between Petrographic Study and XRD Analysis

The two techniques generally have a good correlation. Petrographic study is not possible to identify extremely fine-grained minerals such as illite, sericite, kaolinite, and montmorillonite individually. In contrast, XRD semi-quantitative analysis shows a better detection of mineral composition. However, the XRD technique cannot identify a mineral when it is less than 1% amount from the powder sample.

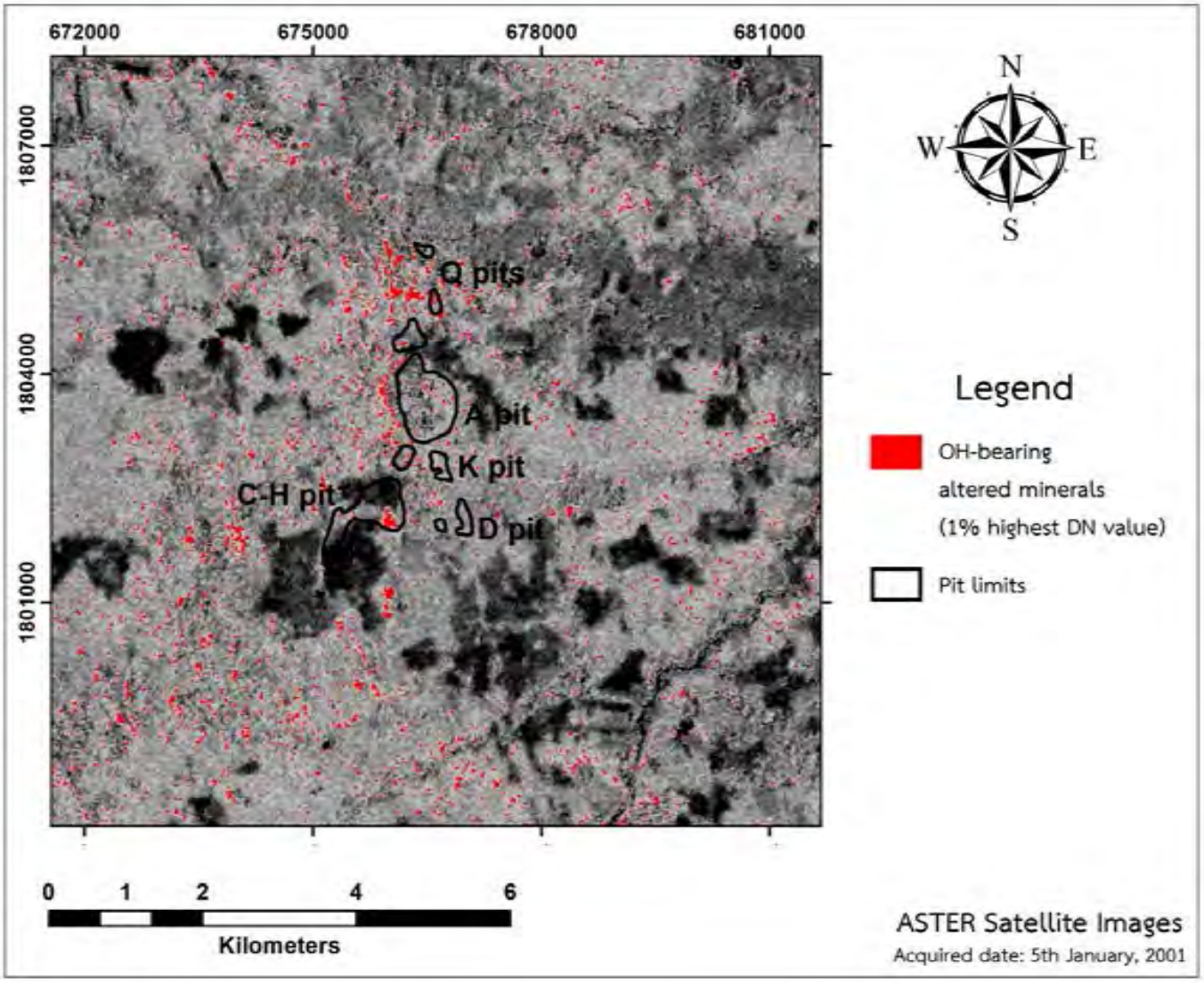

Fig. 5.1 High-potential gold mineralization map from the PC2 with 1% highest DN value showing the OH-bearing altered mineral detection in red with Chatree pit limits.

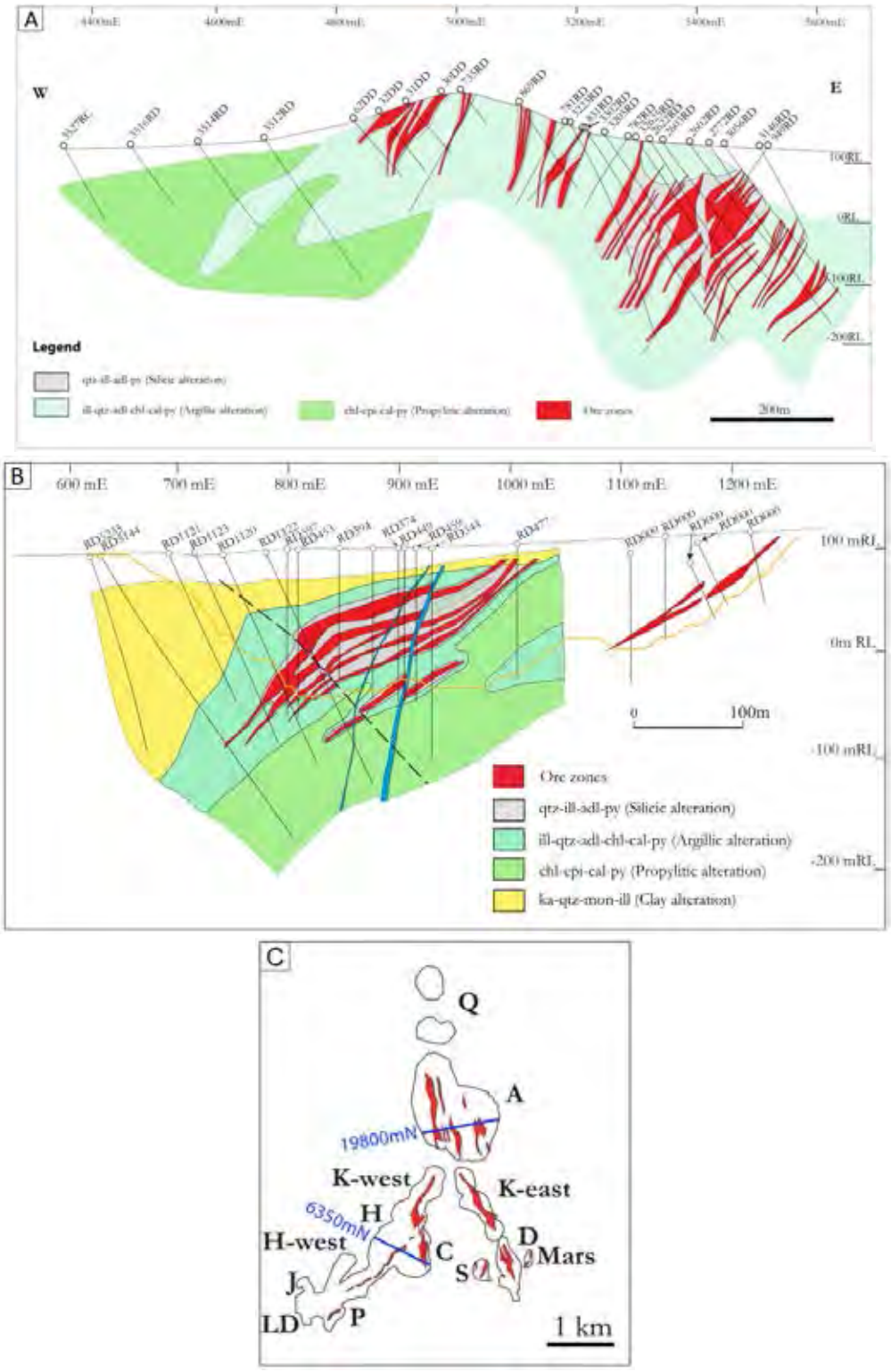

Fig. 5.2 Section 19800mN and 6450mN. **A.** Distribution of A lens alteration zones, **B.** Distribution of C-H lens alteration zones, **C.** The location of cross-section. Mineral abbreviations: qtz = quartz, ill = illite, adl = adularia, py = pyrite, chl = chlorite, cal = calcite, epi = epidote. (Salam, 2013)

5.2 CONCLUSION

ASTER satellite images can be used to detect high-potential gold mineralization areas when analyzed for OH-bearing altered minerals: illite, sericite, chlorite, kaolinite, and montmorillonite. This research can be a case study for detecting high-potential gold mineralization areas for the low-sulfidation epithermal deposit in tropical climates.

5.3 RECOMMENDATION FOR FUTURE WORK

From this study, future work can be studied in using remote sensing techniques for the detection of surface materials:

5.3.1 Using data from different seasons of the year to potentially improve detection in data gathered during the dry season

5.3.2 Using of images from different satellites which have different spectral bands for specific detection on the surface.

REFERENCES

Boloki, M., Poormirzaee, R., 2010. Using ASTER image processing for hydrothermal alteration and key alteration minerals mapping. Proceedings of the 3rd WSEAS International Conference, 77-82.

Crósta, A., De Souza Filho, C.R., Azevedo, F. & Brodie, C., 2003. Targeting key alteration minerals in epithermal deposits in Patagonia, Argentina, Using ASTER imagery and principal component analysis. International Journal of Remote Sensing, 24, 4233–4240.

Diemar, M.G., and Diemar, V.A., 1999, Geology of the Chatree epithermal gold deposit, Thailand: Proceedings of the PACRIM' 99 International Congress, Bali 11-13 October, 227-231.

Elsaid, M., Aboelkhair, H., Dardier, A., Hermas, E., Minoru, U., 2014. Processing of Multispectral ASTER Data for Mapping Alteration Minerals Zones: As an Aid for Uranium Exploration inElmissikat-Eleridiya Granites, Central Eastern Desert, Egypt. The Open Geology Journal 8, 69-83.

Fatima, K., Ur Rehman, A., Khan Khattak, U., Bakhsh Kausar, A., Toqeer, M., Haider, N., 2017. Minerals identification and mapping using ASTER satellite image. Journal of Applied Remote Sensing 11, 1-18.Gabr, S., Ghulam, A., Kusky, T., 2010. Detecting areas of high-potential gold mineralization using ASTER data. Ore Geology Reviews 38, 59-69.

Jensen, J.R., 2005. Introductory Digital Image Processing. Pearson Prentice Hall, Upper Saddle River.

Kromkhun, K., 2005. A Geological setting, mineralogy, alteration, and nature of ore fluid of the H zone, the Chatree deposit, Thailand. M.Sc. thesis. Centre of Excellence in Ore Deposits University of Tasmania.

Loughlin, W., 1991, Principal component analysis for alteration mapping. Photogrammetric Engineering and Remote Sensing 57, 1163–1169.

Lunwongsa, W., Nuanla-ong, S., Charusiri, P. & Sangsir, P., 2011. Alteration study of the Chatree epithermal Au-Ag deposit, central Thailand by a combination of methods; ASD spectrometry, conventional and whole rock ICP geochemistry. International Conference on Geology, Geotechnology and Mineral Resources of Indochina, 89-96.

Ninomiya, Y., 2003. A stabilized vegetation index and several mineralogic indices defined for ASTER VNIR and SWIR data. 2003 IEEE International Geoscience and Remote Sensing Symposium. Proceedings, 1552-1554.

Pour, A.B., Hashim, M., 2012. The application of ASTER remote sensing data to porphyry copper and epithermal gold deposits. Ore Geology Reviews 44, 1-9.

Pour, A.B., Hashim, M., van Genderen, J., 2013. Detection of hydrothermal alteration zones in a tropical region using satellite remote sensing data: Bau goldfield, Sarawak, Malaysia. Ore Geology Reviews 54, 181-196.

Pour, A., Hashim, M., 2014. Integrating PALSAR and ASTER data for mineral deposits exploration in tropical environments: a case study from Central Belt, Peninsular Malaysia. International Journal of Image and Data Fusion, 1-19.

Salam, A., 2013. A geological, geochemical and metallogenic study of the Chatree epithermal deposit, Phetchabun province, central Thailand. Ph.D. thesis. Centre of Excellence in Ore Deposits University of Tasmania.

Salam, A., Zaw, K., Meffre, S., Golding, S., McPhie, J., Suphananthi, S. & James, R., 2008. Mineralisation and oxygen isotope zonation of Chatree epithermal gold-silver deposit, Phetchabun Province, Central Thailand. PACRIM Congress 2008, 1-10.

Salam, A., Zaw, K., Meffre, S., McPhie, J. & Lai, C.-K., 2014. Geochemistry and geochronology of the Chatree epithermal gold–silver deposit: Implications for the tectonic setting of the Loei Fold Belt, central Thailand. Gondwana Research 26, 198-217.

Thompson, A. J. B., Thompson, J. F. H., & Allen, R., 1996. Atlas of alteration: a field and petrographic guide to hydrothermal alteration minerals. St. John's, Nfld, Geological Association of Canada, Mineral Deposits Division.

White, N. & Hedenquist, J., 1995. Epithermal gold deposits. Styles, characteristics and exploration. SEG Newsletter 23, 9-13.

Zhang, X., Pazner, M. & Duke, N., 2007. Lithologic and mineral information extraction for gold exploration using ASTER data in the south Chocolate Mountains (California). ISPRS Journal of Photogrammetry and Remote Sensing 62, 271-282.

Department of Mineral Resources. Geology of Phetchabun Province [Online]. 2008. Retreived December 20, 2017 from http://www.dmr.go.th/download/article/article_20110318134321.pdf

Department of Mineral Resources. Geology of Phichit Province [Online]. 2007. Retreived December 19, 2017 from http://www.dmr.go.th/download/digest/พิจิตร.pdf

Geoimage. The ASTER Sensor [Online]. 2005. Retreived January 15, 2018 from https://www.geoimage.com.au/media/satellite_pdfs/ASTER_Fact-sheet.pdf

APPENDIX A

ASTER SATELLITE IMAGE TRANSFORMATION

A.1 BAND RATIO

The ASTER Level-1B satellite images applied to radiance at the sensor data with atmospheric corrections are transformed with band ratio indices: stabilized vegetation index (StVI), OH-bearing altered minerals index (OHI), kaolinite index (KLI) and calcite index (CLI). The statistical information from each transformed scene is calculated by ENVI software with version 5.1 (Table A.1).

Table A.1 Statistical information of ASTER satellite spatial scenes transformed with band ratio indices.

Band ratio indices	Min	Max	Mean	Standard deviation (SD)
StVI	0	255	113.750761	65.190799
OHI	0	255	102.383039	59.930309
KLI	0	255	91.863841	78.044837
CLI	0	255	115.677193	63.095649

A.2 PRINCIPAL COMPONENT ANALYSIS

The main input parameters for PCA transformation are band ratio indices: StVI, OHI, KLI and CLI applied to ASTER data. The version 10.5 of Esri ArcMap software is used for statistical calculation on imagery covariances and correlation matrix into each principal component (Table A.2-A.4).

Table A.2 Covariance matrix from PCA transformation.

Input band ratio indices	StVI	OHI	KLI	CLI
StVI	0.19814	0.05835	0.00186	0.03659
OHI	0.05835	0.07209	0.02501	0.01545
KLI	0.00186	0.02501	0.02068	-0.00255
CLI	0.03659	0.01545	-0.00255	0.01745

Table A.3 Correlation matrix from PCA transformation.

Input band ratio indices	StVI	OHI	KLI	CLI
StVI	1	0.48816	0.02908	0.6222
OHI	0.48816	1	0.64768	0.43544
KLI	0.02908	0.64768	1	-0.13399
CLI	0.6222	0.43544	-0.13399	1

Table A.4 Eigenvalues and Eigenvectors from PCA transformation.

Input band ratio indices	StVI	OHI	KLI	CLI	Eigenvalues	Eigenvalues (%)
PC1	0.91137	0.36495	-0.22707	-0.00292	0.22898	74.2546
PC2	-0.34326	0.80689	0.25001	-0.39145	0.06157	19.9675
PC3	-0.22707	0.47979	-0.53469	0.69386	0.01347	4.3676
PC4	-0.00292	-0.02987	0.77463	0.60442	0.00435	1.4103

APPENDIX B

X-RAY DIFFRACTION PATTERNS

The oriented XRD powder samples of the study area were analyzed by x-ray diffraction instrument (Table B.5). The analysis results show the mineral composition and their crystallographic orientation in the samples (Fig. B.1-B.12). The amount of preferred mineral can be indicated by the areas under each mineral's peak on EVA software.

Table B.1 XRD instrument used for oriented powder samples' analysis.

TOPIC	DESCRIPTION
Analytical Instrument	X-Ray Diffractor Model D8 Advance: Bruker AXS, Germany
Target/Wavelength	Cu/1.5406
Voltage/Current	40 kV/30 mA
Conditions	2-theta 5°-30°, increment of 0.02°, Scan speed at 1 sec/step
Program used	Diffrac Plus software of the Bruker Analytical X-ray System (XRD Commander)
Interpreted using	EVA Program which search-map based on the samples' Powder Diffraction File (PDF) and compared with to JCPDS's reference PDF database

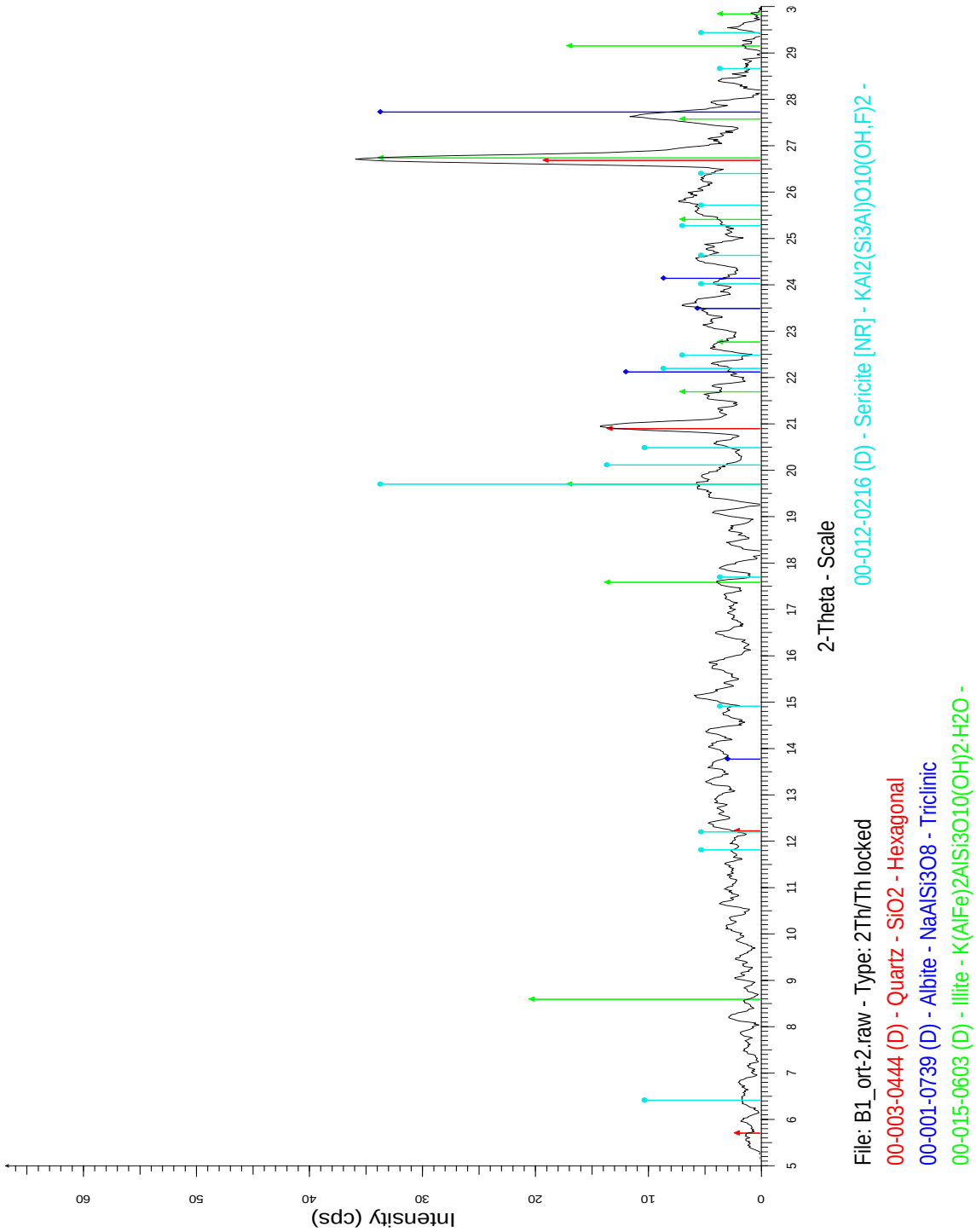

Fig. B.1 Diffraction pattern of sample B01 taken from B-prospect area.

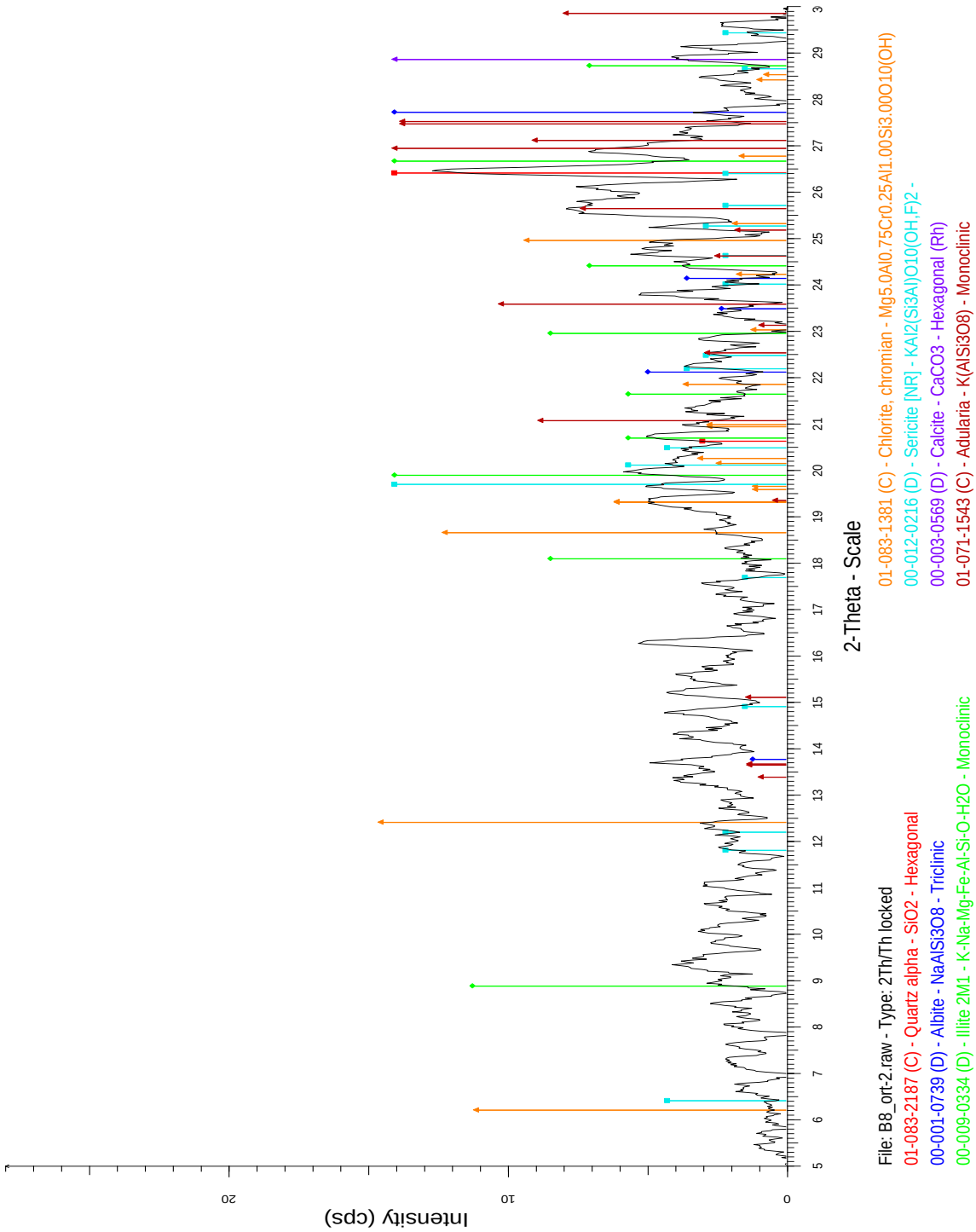

Fig. B.2 Diffraction pattern of sample B08 taken from B-prospect area.

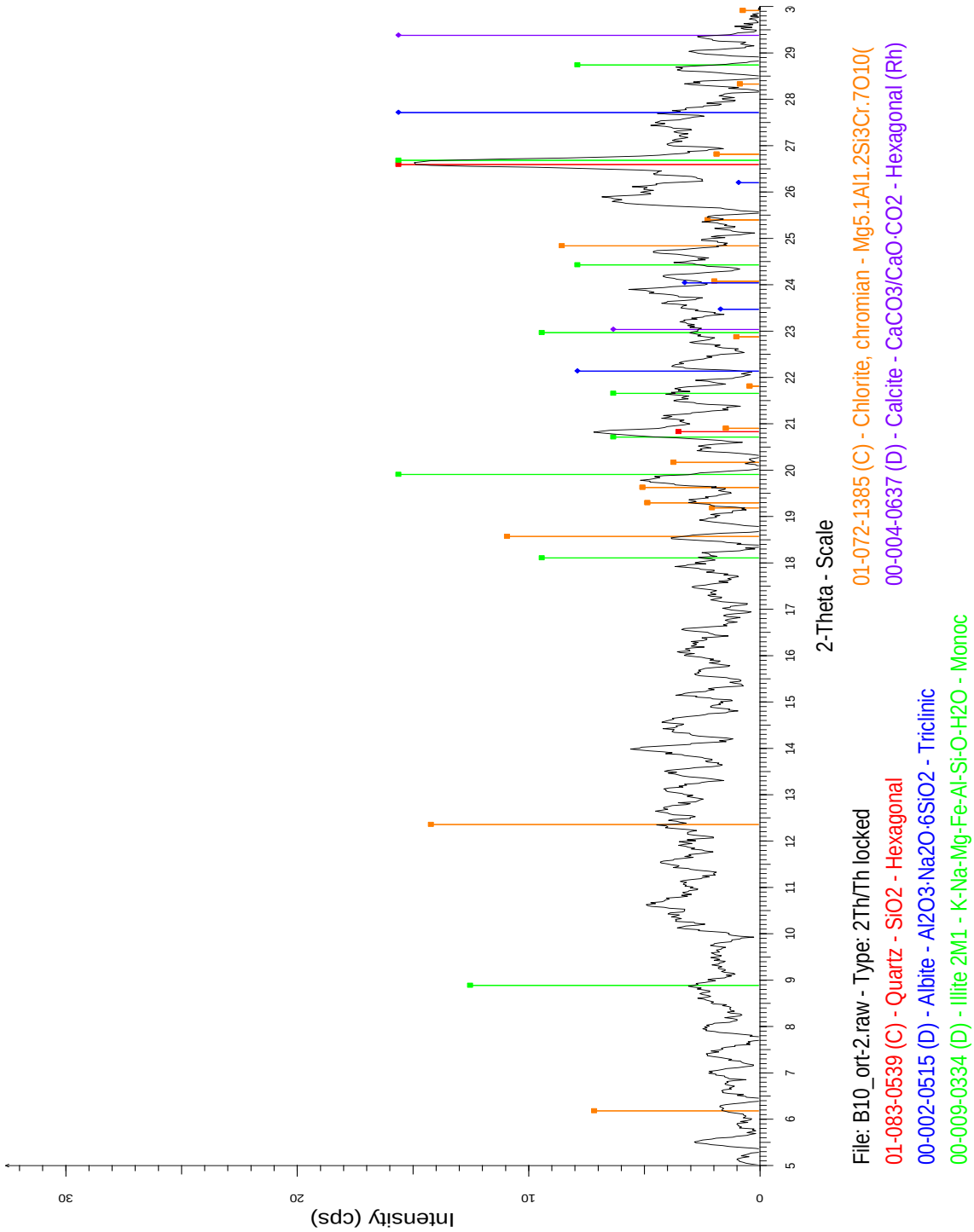

Fig. B.3 Diffraction pattern of sample B10 taken from B-prospect area.

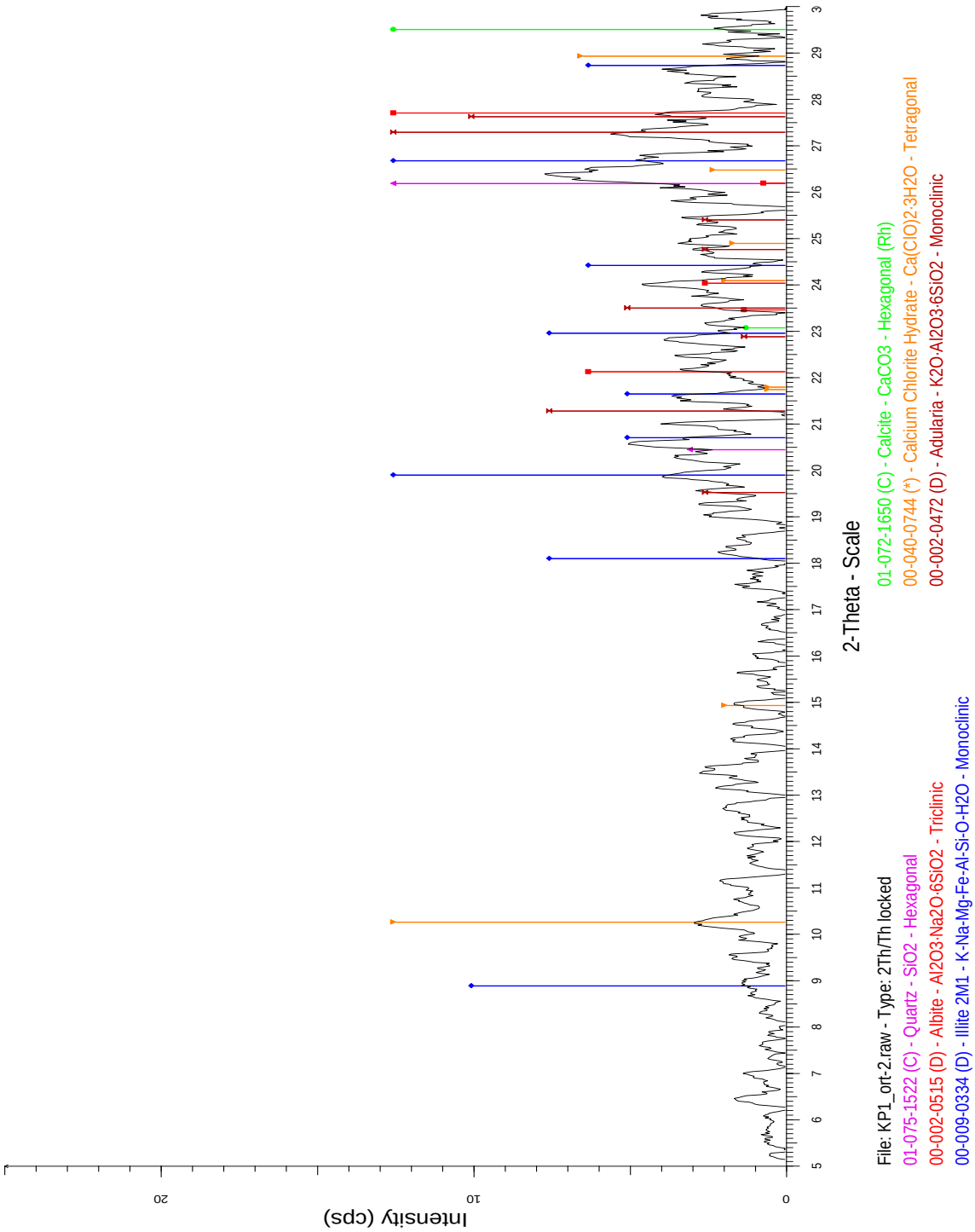

Fig. B.4 Diffraction pattern of sample KP01 taken from Khao Pong area.

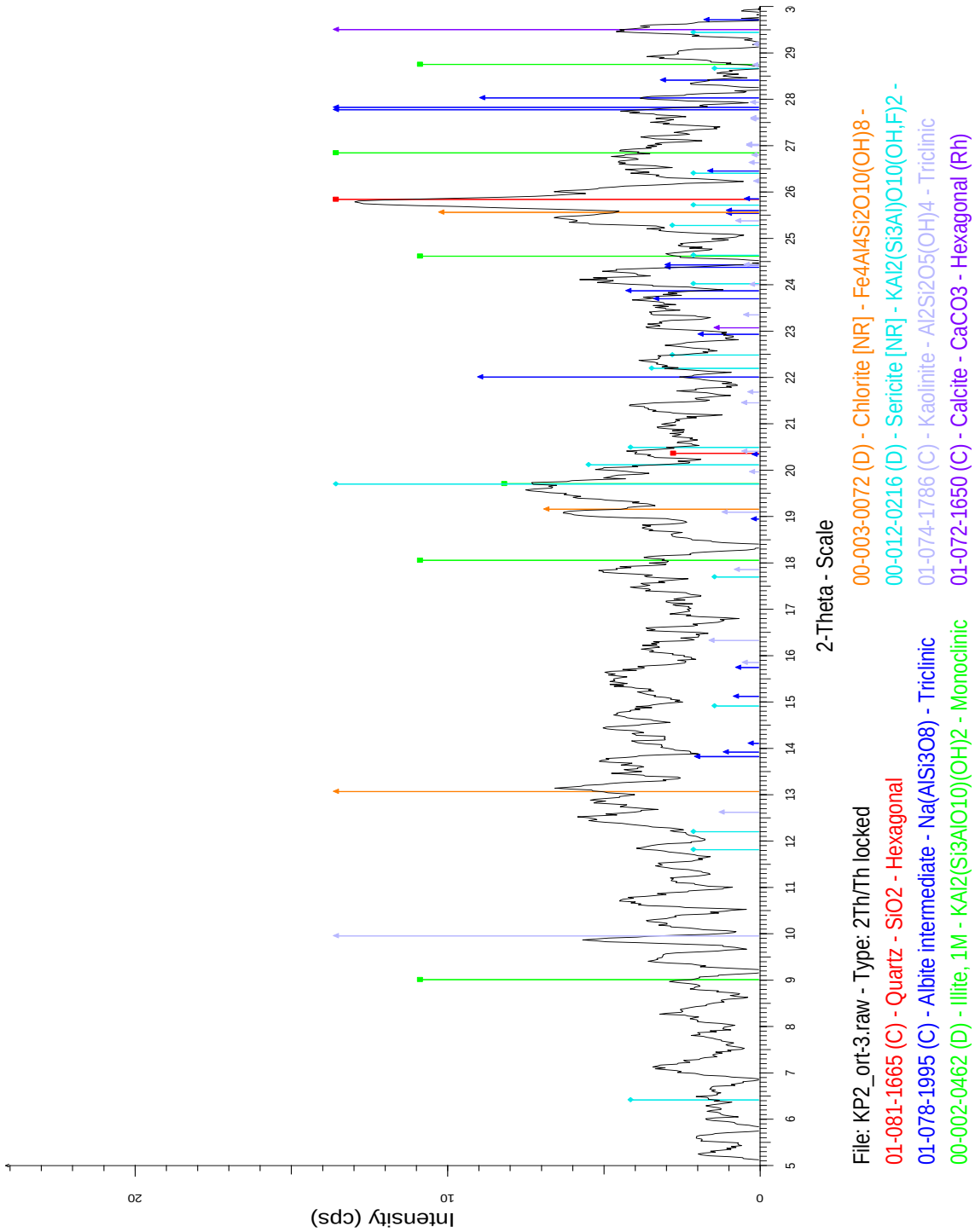

Fig. B.5 Diffraction pattern of sample KP02 taken from Khao Pong area.

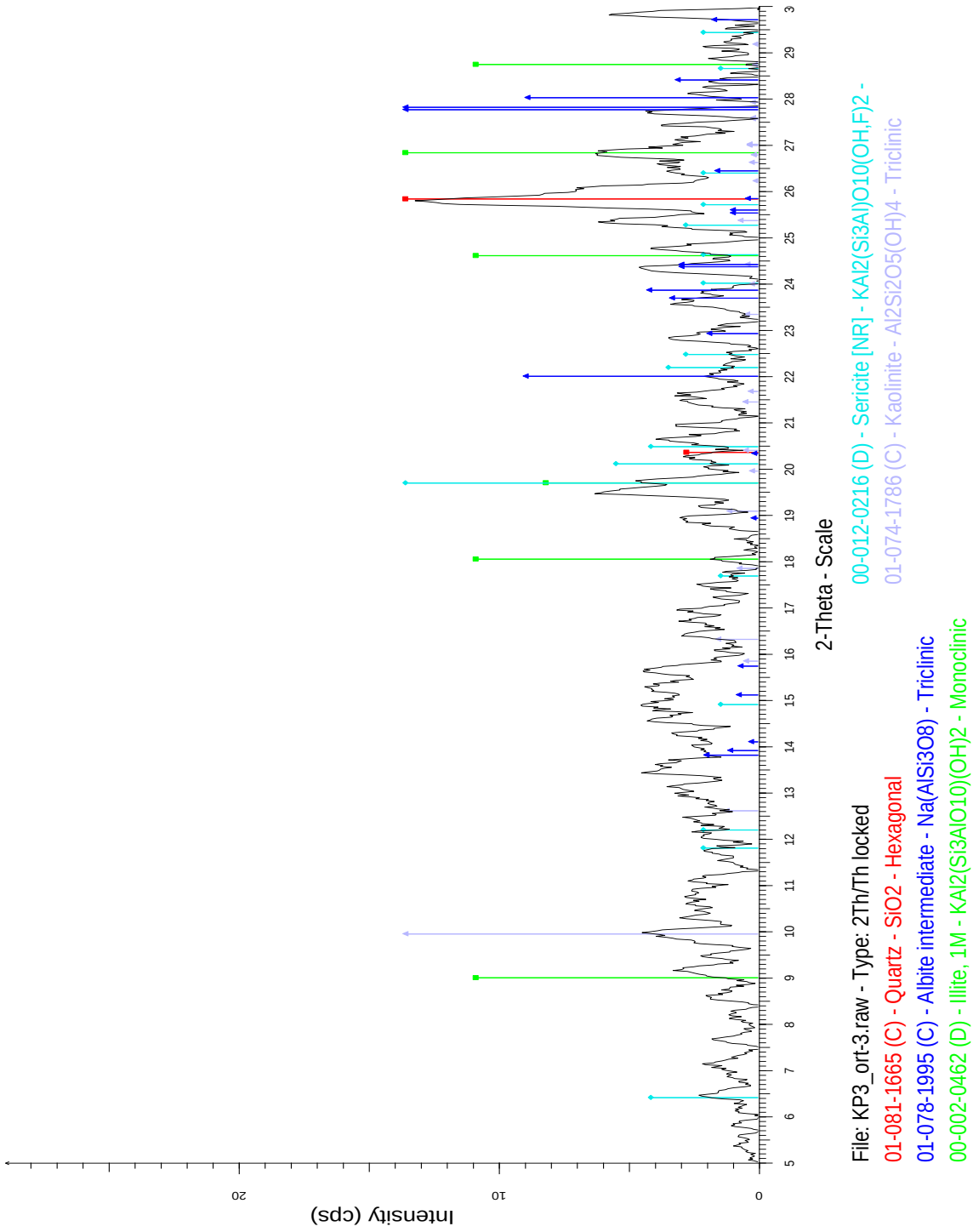

Fig. B.6 Diffraction pattern of sample KP03 taken from Khao Pong area.

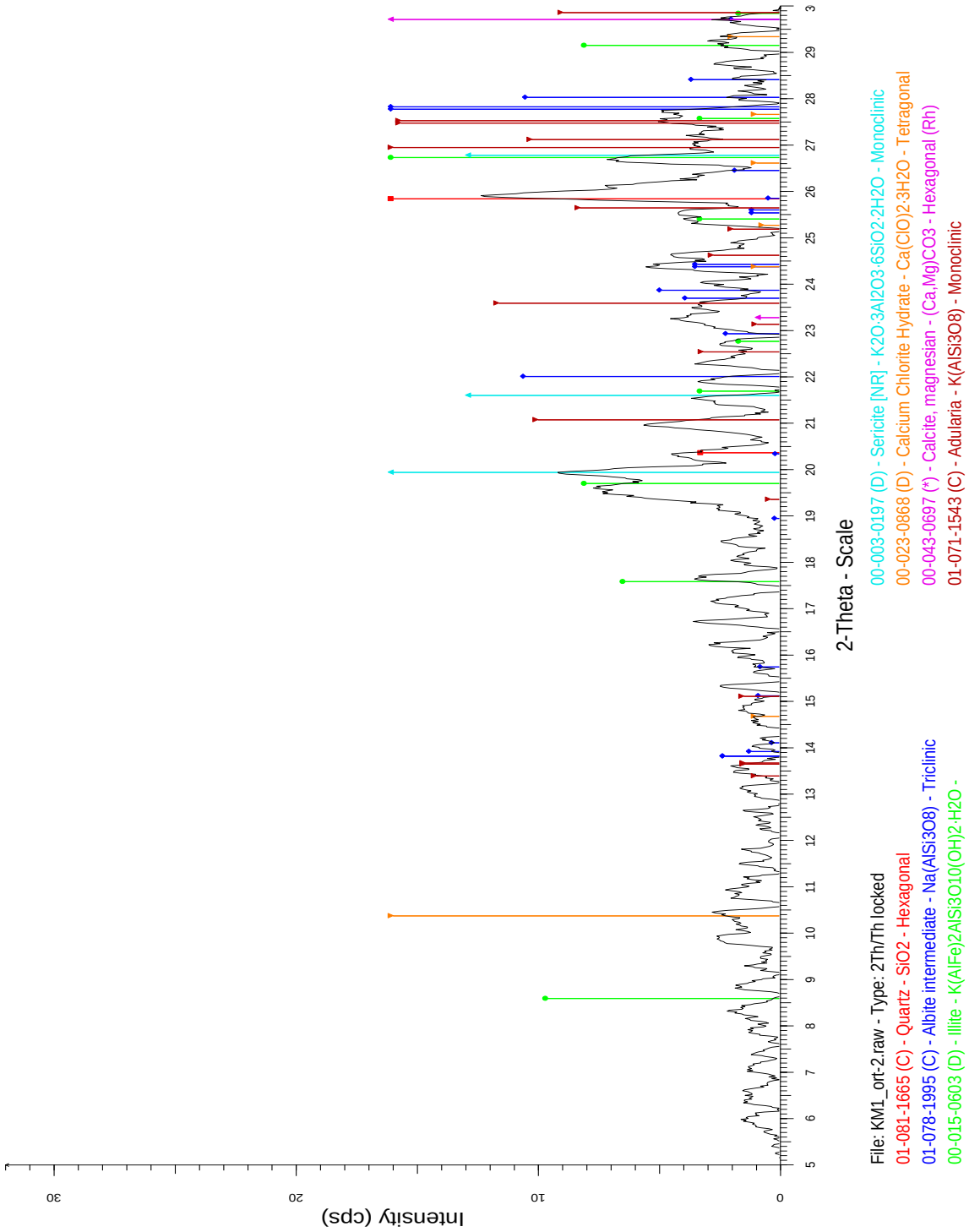

Fig. B.7 Diffraction pattern of sample KM01 taken from Khao Mo area.

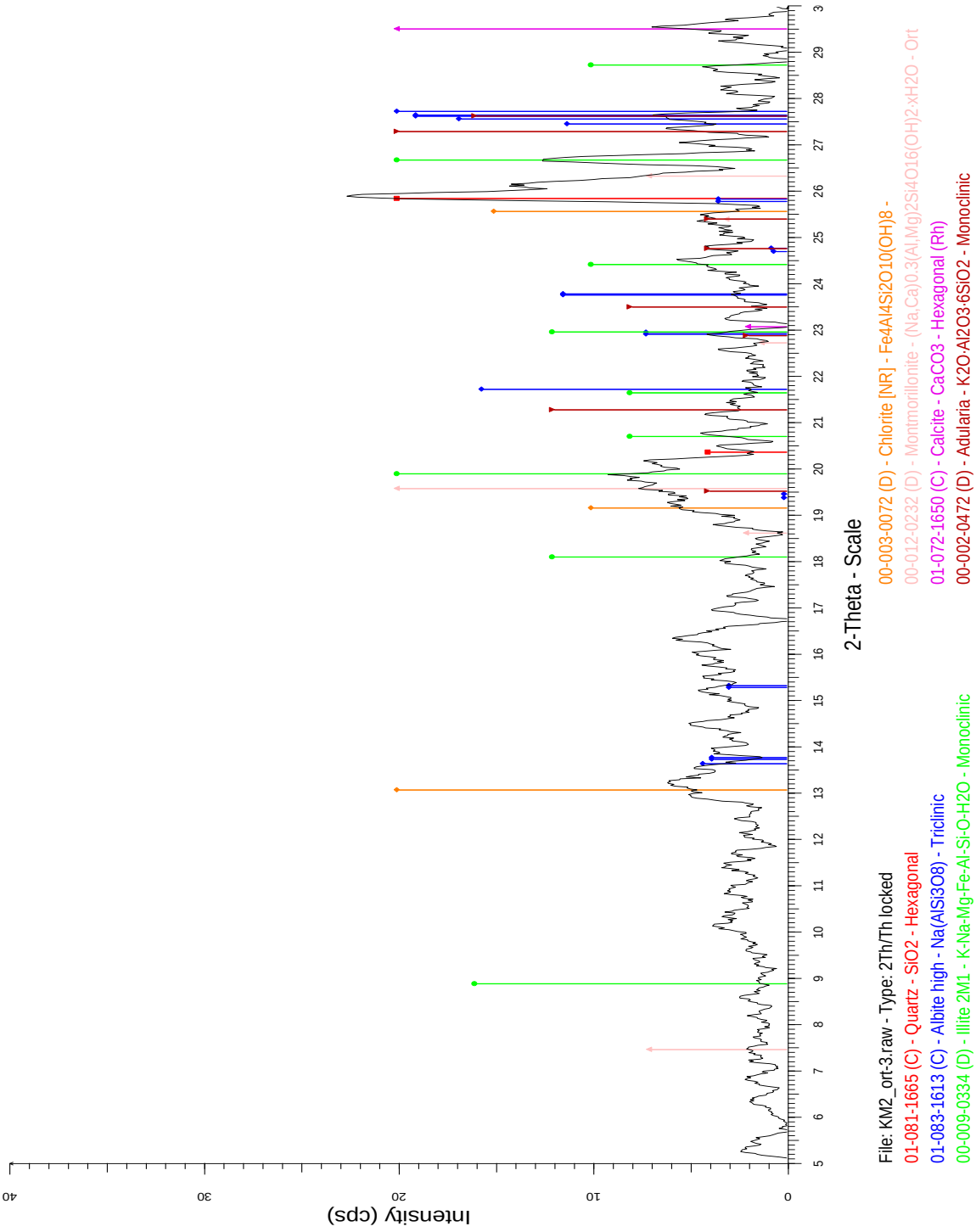

Fig. B.8 Diffraction pattern of sample KM02 taken from Khao Mo area.

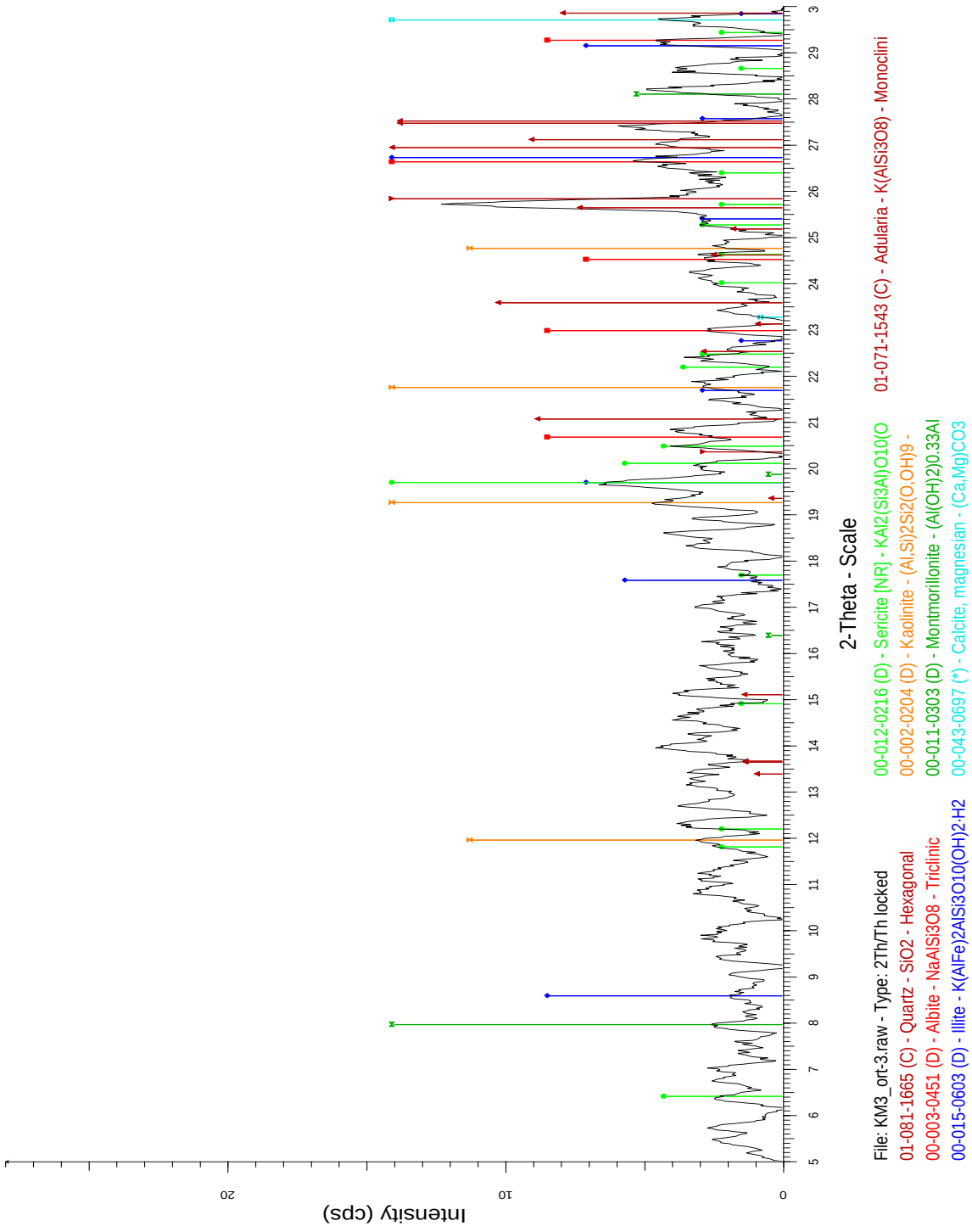

Fig. B.9 Diffraction pattern of sample KM03 taken from Khao Mo area.

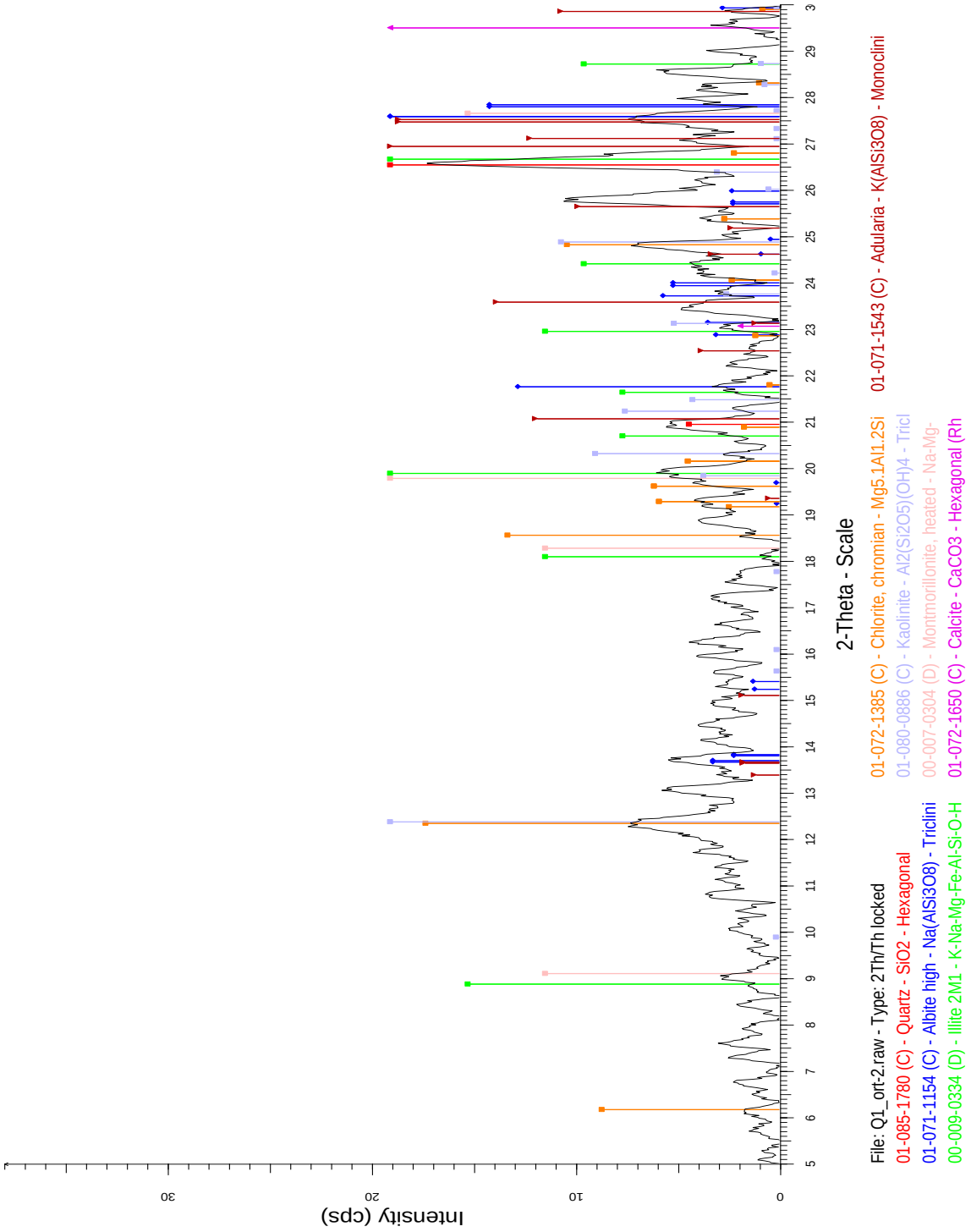

Fig. B.10 Diffraction pattern of sample Q01 taken from Q pit area.

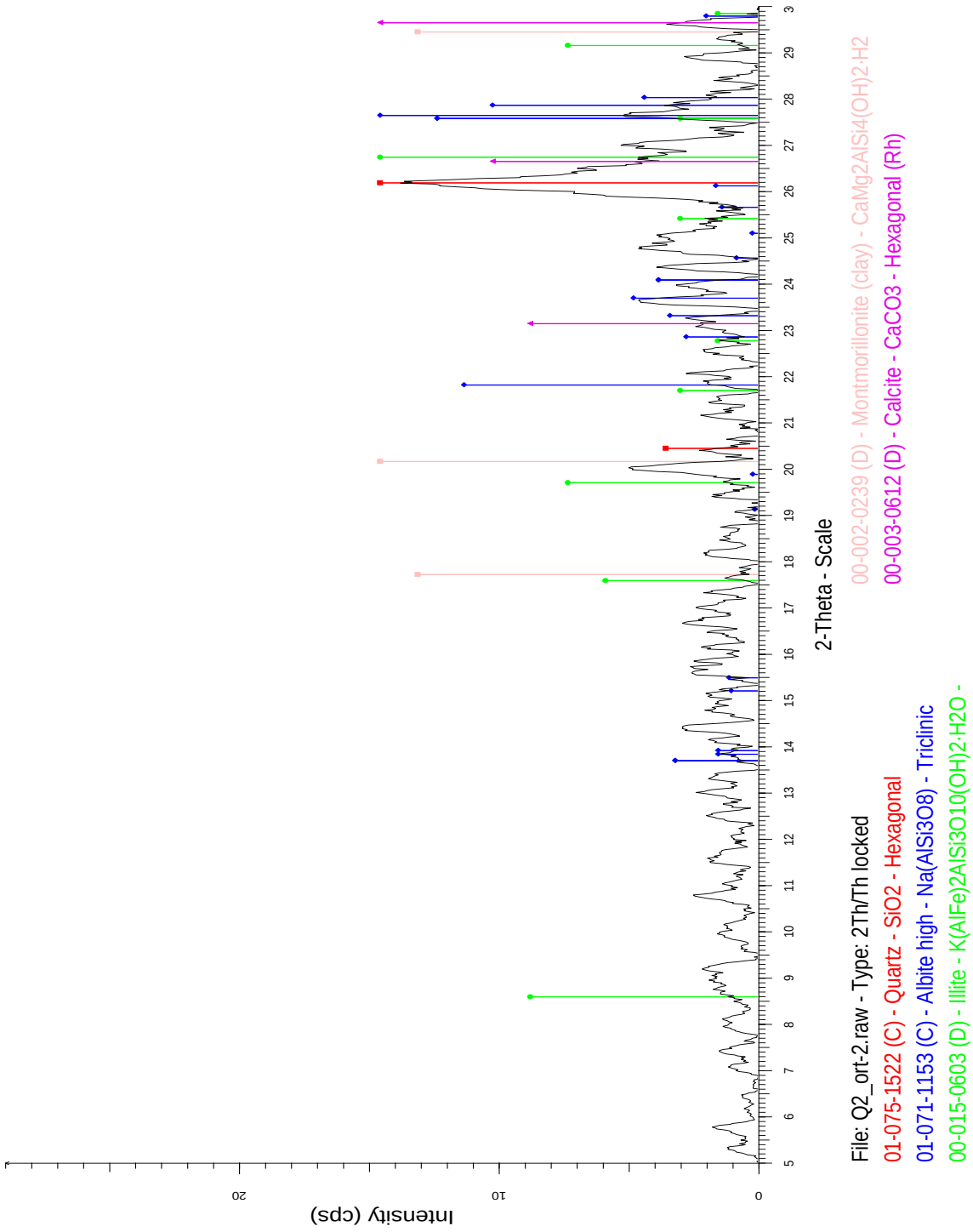

Fig. B.11 Diffraction pattern of sample Q02 taken from Q pit area.

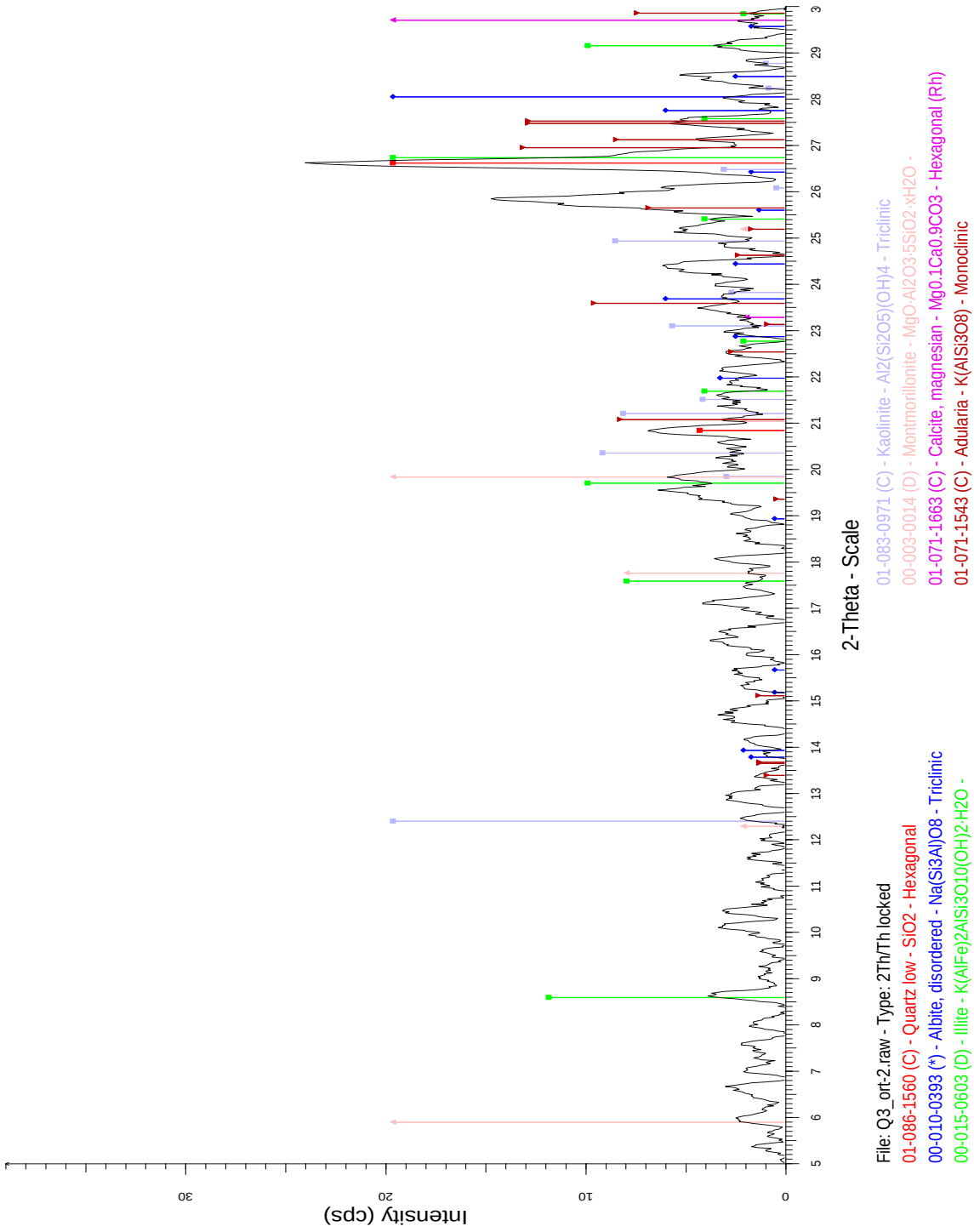

Fig. B.12 Diffraction pattern of sample Q03 taken from Q pit area.